NASA Technical Paper 2572

March 1986

NASA-TP-2572 19860010989

# Star 48 Solid Rocket Motor Nozzle Analyses and Instrumented Firings

Robert L. Porter



NASA

NASA
Technical
Paper
2572

1986

# Star 48 Solid Rocket Motor Nozzle Analyses and Instrumented Firings

Robert L. Porter

*George C. Marshall Space Flight Center*
*Marshall Space Flight Center, Alabama*

NASA
National Aeronautics
and Space Administration

Scientific and Technical
Information Branch

## TABLE OF CONTENTS

# LIST OF ILLUSTRATIONS

TECHNICAL PAPER

# STAR 48 SOLID ROCKET MOTOR NOZZLE ANALYSIS AND INSTRUMENTED FIRINGS

## INTRODUCTION

Failures and anomalies in several NASA, DOD, and U.S. industrial solid rocket motor programs have identified a need for more knowledge in the areas of nozzle materials, design analyses, manufacturing, and component quality assessment. The George C. Marshall Space Flight Center (MSFC) has been authorized by the NASA Headquarters to perform research and technology programs to obtain and provide an expanded and improved nozzle design data base for use by the U.S. solid rocket motor industry.

This document discusses the analysis and instrumented testing conducted to date. The nozzle selected for analyses and testing was a Star 48 manufactured by the Morton Thiokol, Elkton Division. The Star 48 is an upper stage motor with a history of two flight failures on February 3 and 6, 1984, and a ground failure in December 1980. Initial failures of the nozzle occurred within the first 10 sec of motor firing.

Following the ground test failure, Prototype Development Associates (PDA) completed a thermal/structural analysis in 1981 [1] for Morton Thiokol which showed a marginally designed exit cone.

Beginning in August 1984, MSFC has performed thermostructural analyses and there have been two short duration sea-level motor firings designated carbon/carbon technology (CCT)-1 and carbon/carbon technology (CCT)-2. This paper describes the configurations for the two nozzles, the analyses performed by MSFC, the instrumentation, the analysis and test results, and the conclusion reached from the analysis and the motor firings. Nozzle instrumentation and motor firings were conducted by Morton Thiokol/Elkton Division under contract to MSFC.

## CONFIGURATION

The STAR 48 motor has a titanium motor case with a nozzle as shown in Figure 1. The nozzle consists of a three-dimensional (3D) carbon/carbon integral throat exit (ITE) with a tape wrap carbon phenolic nose cap and a titanium closure that is bolted to the aft bulkhead of the motor case. The two-dimensional carbon/carbon involute exit cone is threaded to an involute carbon phenolic insulator. The carbon phenolic insulator is connected to a titanium adapter which is threaded to the titanium closure. The flight nozzle contains C-34 cement between the exit cone and insulator including the forward thread of the exit cone and insulator. Also, the carbon/carbon exit cone is pinned to the carbon phenolic insulator at the connecting threads with four radially-oriented silica pins located 90 deg apart. These pins are used to prevent rotation or loosening of the exit cone. The chamber pressure loads on the nose cap and ITE are transmitted through an involute-constructed carbon phenolic "Dixie Cup" to the titanium closure. The interface gap between the exit cone and dixie cup is filled with zinc chromate putty. O-rings are used at the interface of the exit cone and insulator forward of the thread at the forward end of the insulator and titanium closure interface. The STS configuration exit cone is 34.2 in. long.

The first nozzle firing test (CCT-1) was a baseline configuration with minimum clearance between the exit cone and insulator (nominal clearance is 0.010 in.) and a maximum amount of C-34 cement in the gap between the two parts. The CCT-1 nozzle exit cone was cut off to a length of 19.0 in., as shown in Figure 2. The second nozzle firing test (CCT-2) had a maximum gap and C-34 cement applied only to the aft 1-1/4 in. of exit cone to insulator interface with 21, 1/2 in. wide voids or vent paths. Also, the exit cone was cut to a length of 9.5 in. as shown in Figure 2, and a heat shield was added as shown in Figure 3. The reason for the shorter exit cone was due to an exit cone buckling failure on CCT-1 aft of the insulator caused by sea-level testing. This failure will be addressed later.

## ANALYSIS

The most extensive thermal and stress analysis of the nozzle performed prior to the two flight failures in early February 1984 was by PDA Engineering. This analysis was performed following a ground test failure designated DM-2 in December 1980. After the two flight failures, PDA Engineering performed additional thermostructural analysis in support of the failure investigation. Both of these nozzle analyses excluded the ITE and nose cap, since the loads from these parts are transmitted to the titanium closure and since they were designed not to interact with the exit cone. The latter analysis showed high stresses in the exit cone at three locations as shown in Figure 4. The critical time was 3 to 7 sec.

Beginning in July 1984, MSFC obtained a newly developed thermostructural analysis code called the Champion code. The Champion code was developed for the U.S. Navy. This stress analysis code is an incremental code which automatically uses the resulting data from one computational time slice as input to the next time slice. Due to the urgency of obtaining results, a thermostructural analysis was performed using the PDA engineering two-dimensional (2D) model, material properties, and predicted temperatures. Analyses were performed for the first 10 sec of motor burn. The stress model contained 1707 nodes and 1585 “higher order” elements.

Several modifications were made to the Champion code while performing analyses for the CCT-1 and CCT-2 configurations. These changes included adding a capability for modeling involutes. This change allows the user to input material properties in the material directions (warp, fill, and cross-ply), instead of the global coordinates (radial, hoop, and axial). Also, the stresses are available in the material directions and the global directions. Another addition to the code was the ability to obtain margins of safety for stresses and strains in the material directions.

Although no single acceptable failure criteria has been established for carbon/carbon and carbon phenolic materials, a failure capability was added to the Champion code. This failure criteria is based on uniaxial strain and it allows the stress at an integration point to decrease to zero when the ultimate strain is reached in a particular material direction. This failure criteria was chosen for convenience and is not based on test data. However, this is believed to be a more realistic approach than allowing both the stresses and strains to continue to increase after the ultimate strain is reached.

### A. CCT-1 Thermostructural Analysis

A stress analysis was made using the Champion code for the CCT-1 nozzle configuration discussed earlier and predictions were made for the CCT-1 motor firing conducted in December 1984. The CCT-1 analysis included motor chamber pressure and temperatures supplied by PDA Engineering. The analysis revealed negative margins of safety on some elements in the carbon/carbon exit cone. Analysis results were printed for 1.0, 2.0, 3.0, 5.0, 7.0, and 10.0 sec.

Strain gage locations were chosen which corresponded to node locations in the stress model. The stress analysis included very stiff interface elements between the exit cone and the exit cone insulator. This analysis did not address the charring of C-34 cement in the interface. Some nodal temperature discrepancies or anomalies were observed, which were judged not significant in the critical stress locations. The temperature anomalies resulted from transferring temperatures from the thermal model to the stress model.

### B. CCT-1 Buckling Analysis

Following the CCT-1 test and an exit cone failure aft of the insulator, a buckling analysis of the exit cone was performed. Using a nozzle pressure profile as shown in Figure 5, a buckling analysis was performed which confirmed the buckling failure. This failure was due to flow separation in the nozzle and the external sea-level pressure. This condition does not exist in flight or during an altitude test and is not related to the ground test failure or the two flight failures. The buckling analysis was performed using the SPAR computer code. An equivalent isotropic modulus was calculated using the orthotropic moduli. This buckling analysis is described in detail in Reference 3.

### C. CCT-2 Thermostructural Analysis

A thermostructural analysis was performed for the CCT-2 nozzle configurations using the same temperatures as used in the CCT-1 analysis. The analysis took into account the 0.010 gap between the exit cone and insulator, but it did not consider any bondline pressure. The influence of bondline pressure was omitted because the CCT-2 configuration contained vent paths to prevent any gas pressure. The CCT-2 analysis showed lower stresses in the exit cone aft of the thread and some increase in stresses forward of the threads in certain material directions. Also, the analysis showed that a gap increase beyond the 0.010 in. would not affect the analysis results for the first 10 sec of motor burn. Strain predictions were provided for the CCT-2 test for all strain gage locations. Again, negative margins of safety were calculated for certain material directions. Most negative margins of safety occurred in the cross-ply direction. Uncertainty in the material properties is largely responsible for the negative margins of safety. Updated temperatures were extrapolated from the previous thermal analysis, and used in the stress analysis for the CCT-2 configuration.

## INSTRUMENTATION

### A. CCT-1 Instrumentation

The instrumented CCT-1 nozzle assembly contained 28 thermocouples on the exit cone, 22 on the exit cone insulator, and eight on the closure for a total of 58. In addition, there were 12 strain gages on the exit cone, 38 on the exit cone insulator, and 16 on the closure for a total of 66. There were eight pressure measurements to monitor the C-34 bondline pressure between the exit cone and the exit cone insulator. The pressure measurements were made at four circumferential locations and two axial locations. The instrumentation locations are shown in Figure 6. Some of the strain gages were uniaxial gages while others were biaxial gages. The strain gages used were EA-06-125-TM-120 and CEA-06-500UW-120. Strain measurements were taken at four circumferential positions at each of the axial locations.

### B. CCT-2 Instrumentation

The instrumentation plan for CCT-1 was changed for the CCT-2 test. A description of the instrumentation is shown in Figure 7 and tabulated in Table 1. The CCT-2 instrumentation plan, in general, provides for more axial locations with fewer circumferential positions at each axial location. The CCT-2 instrumented nozzle assembly contained 28 thermocouples on the exit cone, 23 on the exit cone insulator, and 8 on the closure for a total fo 59. Additionally, there were 23 strain gages on the exit cone, 38 on the exit cone insulator, and 7 on the closure for a total of 68. There were also 4 pressure measurements at 2 axial locations for a total of 8. These pressure measurement locations were the same as those for the CCT-1 nozzle; however, the installation of the CCT-2 nozzle pressure measurements was improved due to problems with the CCT-1 installation.

## TEST RESULTS

These tests provided valuable data for the thermal and structural response characterization of the nozzle components, and provided new insight to earlier nozzle failures. Both motor tests were configured to provide 10 sec of motor operation with a mass flow of 50 lb per second. Both motor tests were conducted at sea-level under nonspin and ambient (50° to 70°F) temperature conditions. Also, both tests included a post-test quench system to minimize the effects of post-fire heat soak through the heat affected and virgin materials. The quench was very successful on each motor test.

During the CCT-1 test, the exit cone failed at 0.53 sec. This failure was detected by cameras and several strain measurements. As a result of this failure, some measurements were lost earlier than expected due to instrumentation leads being exposed to heat.

Test data from CCT-1 and CCT-2 are included in appendixes A and B, respectively. This data includes pressure, temperature, and strain plots. Predicted temperatures and strains are plotted along with the measured data.

From the CCT-1 bondline pressure data and post-test hardware evaluation, it was concluded that the pressures were higher than those measured. Although adhesive was used to isntall the pressure tubes, it blew out during firing which caused gas leakage. This was verified by post-test hardware inspection. Improvements in installation of pressure measurements were made for the CCT-2 test, and good pressure data was obtained through motor test and post-test cooldown. Bondline pressures at the forward location for CCT-2 exceeded 400 psi, even with the 21, 1/2 in. wide vents between the exit cone insulator. No bondline pressure had been included in the nozzle design. This bondline pressure increases the compressive stresses in the exit cone and produces a significant axial force that must be reacted through the threads in the carbon/carbon exit cone and the carbon phenolic exit cone insulator.

The peak pressure measured at the aft location for the CCT-2 test was below 300 psi. The difference in the pressure measurements at the forward and aft location is due to the bondline gap locally closing between the two locations. Also, the pressures were still increasing at the end of motor burn. The effect of chamber pressure on bondline pressure at the forward location can be seen by a sudden decrease in bondline pressure at 11.5 sec (i.e., 1.5 sec after shutdown).

Post-test hardware inspection of CCT-1 and CCT-2 showed an aft shift of 0.02 in. in the exit cone with respect to the exit cone insulator. This exit cone shift had been observed on hardware after full length test, but it was believed to occur late in motor burn.

As can be seen from the plots, the test temperatures of the exit cone at the E-1 and E-9 locations were much lower than predicted. The measured axial and hoop strains were quite different from the predicted strains at the E-1 location. The E-1 hoop strain reversals at 1.0 sec and 2.5 sec and the E-1 axial strain reversal at 2.5 sec are not understood. These reversals could be caused by unknown loads, the shift in the exit cone or some kind of strain response associated with the carbon/carbon involute cone. Additional laboratory tests and motor tests are planned to further understand the data and nozzle behavior.

All the exit cone strain gages were lost, as expected, early due to temperature. A compromise was made on the strain measurements due to a limited number of data channel, data on key nozzle components, and the expected time of good data.

No specific strain responses were observed due to the bondline pressure; however, the strain gages most sensitive to the bondline pressures (I-5, I-6, and I-7) were lost shortly after the bondline pressure began to increase. No insulator (I-2) or aft closure (C-2) strain gage shows a response that can be attributed to the interface pressure; however, the effect of motor chamber pressure can be seen on these gages at these locations.

## STRAIN GAGE MEASUREMENTS

### A. Exit Cone

Almost all strain gages mounted in the hoop direction, regardless of axial locations, exhibit a similar type of response of strain versus burn time, although not at the same time. Each hoop strain increases, then decreases, and then increases again. This trend was observed on CCT-1 and CCT-2 tests. Some of the strain data from CCT-1 was questionable at first due to the aft exit cone failure. After evaluating the CCT-2 strain data, it was obvious that the CCT-1 strain data was better than originally believed. It was observed that the E-1 hoop strain was greater at 1.0 sec on CCT-2 than on CCT-1.

### B. Exit Cone Insulator

The E-1 axial compressive strains were greater on CCT-2 than on CCT-1. The SI-2 strain gage showed the effects of chamber pressure. The SI-2 hoop strain showed compressive strain initially with the thermal loads over coming the chamber pressure loads at about 3.0 sec. Some difference was observed in the CCT-1 and CCT-2 hoop strains, but there were some variations in the circumferential locations for each nozzle can be expected regardless of the bondline gap.

### C. Closure

The SC-2 axial strains were larger on CCT-1 than those on CCT-2. At 5.0 sec, the C-2 compressive axial strain on CCT-1 was 900 micro-inches per inch while the C-2 compressive axial strain on CCT-2 was 700 micro-inches per inch. The C-2 hoop strains returned to zero earlier on CCT-1 (8.0 sec) than on CCT-2 (later than 10.0 sec).

## CONCLUSIONS

The CCT test program has provided significantly more thermal and strain data on the nonmetallic components of a nozzle than has been accumulated in solid rocket motor test to date. The number of strain measurements on the nonmetallic materials is believed to be an order of magnitude greater than those on any other nozzle during a motor firing. Until this test program was conducted, all emphasis was placed on the design, manufacture, and inspection of the carbon/carbon exit cone (i.e., ply pattern, density, C-scan, and low density indications). These motor test firings confirmed high interface pressures which had never been considered in the thermostructural analysis. Also, much larger vent area is needed to eliminate the bondline pressure. Additionally, the aft shift in the exit cone occurs earlier in burn time than previously expected, and the shift results from plastic deformation of the carbon phenolic insulator. The shearout of the carbon phenolic insulatir is a credible failure mode not addressed prior to the CCT test program. The exact time of the aft shift of the exit cone is unknown, but future tests will try to determine the time. The axial loads on threads are due to the axial component of the bondline pressure load, and possibly axial loads being introduced on the forward end of the exit cone by the ITE or the zinc chromate putty. Other unexpected results of the tests were the exit cone strain reversals.

Results of these tests and analyses suggest that several simple improvements can be made to improve the Star 48 nozzle. Some improvements are: (1) put axial grooves in the carbon phenolic exit cone insulator to vent the bondline pressure, (2) add more radial pins in the exit cone/insulator threads, (3) improve exit cone ply pattern, and (4) provide additional clearance between the ITE and exit cone.

These tests proved that the nonmetallic components of a nozzle can be instrumented with thermocouples and strain gages without compromising the test. Since the calculated minimum margins of safety occur early in motor operation, short tests are desirable to provide maximum test data to verify analytical models and margins of safety.

These technology tests and analyses represent a very significant step toward developing test technology and analytical capability, and understanding the operational structural characteristics and verifying margins of safety of solid rocket motor nozzles with carbon/carbon involute exit cones.

# REFERENCES

1. Crose, James G., and Miyazawa, Eugene T.: Thermostructural Analyses of the Star 48 Carbon-Carbon Involute Exit Cone. Prototype Development Associates, PDA TR-5651-00-01, September 1981.

2. Ehrenpreis, D., Haisler, W., and Benedicto, R.: 3-D Mathematical Model for Motor Stress Analysis. Naval Weapon Center, China Lake, California 93555, March 1984.

3. Sullivan, Roy M.: Hydroburst Test of a Carbon-Carbon Involute Exit Cone. August 1985.

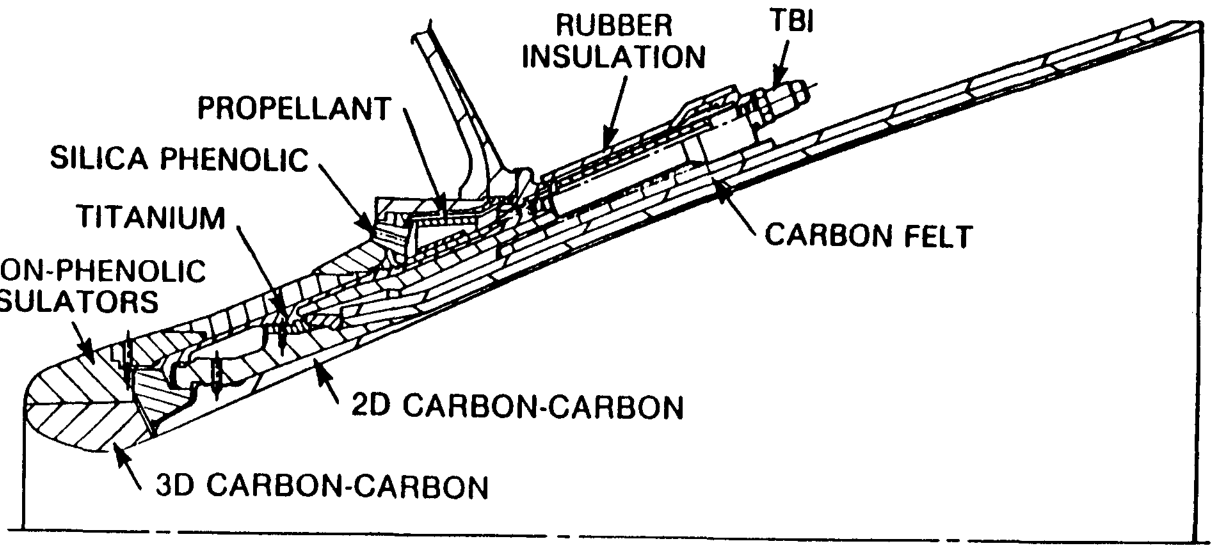


Figure 1. Star 48 nozzle assembly with carbon/carbon exit cone.

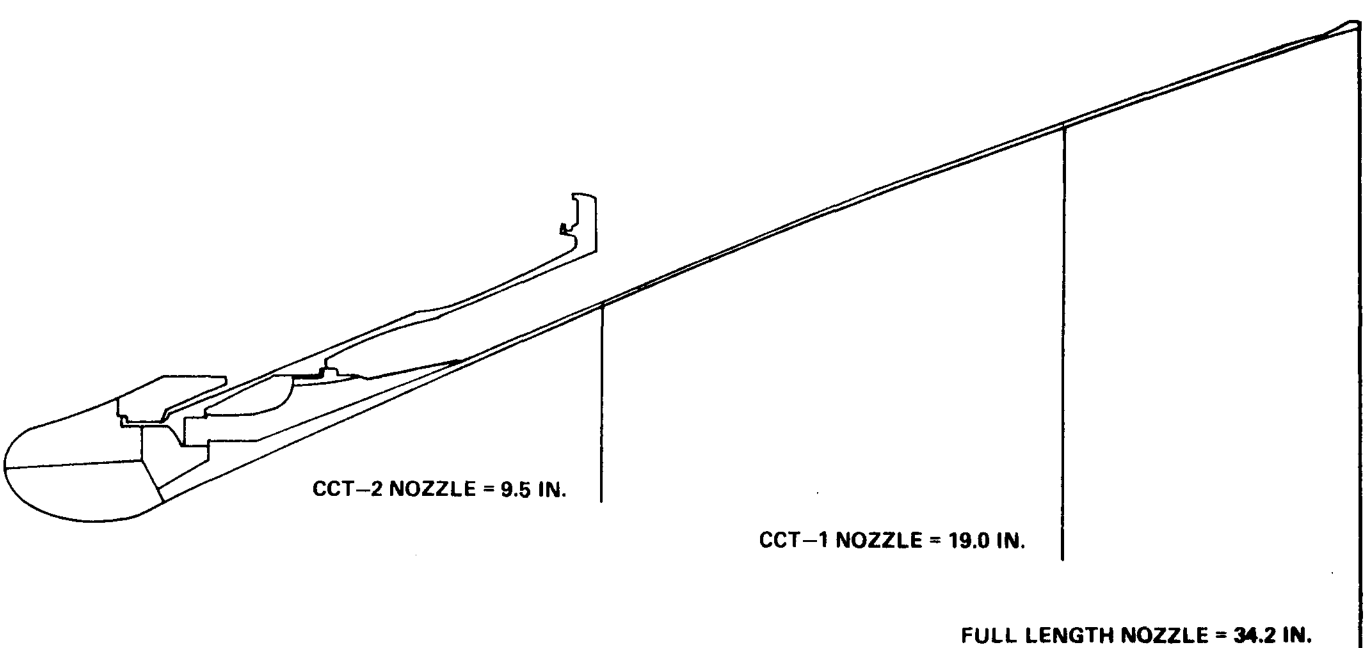


Figure 2. Nozzle length comparison.

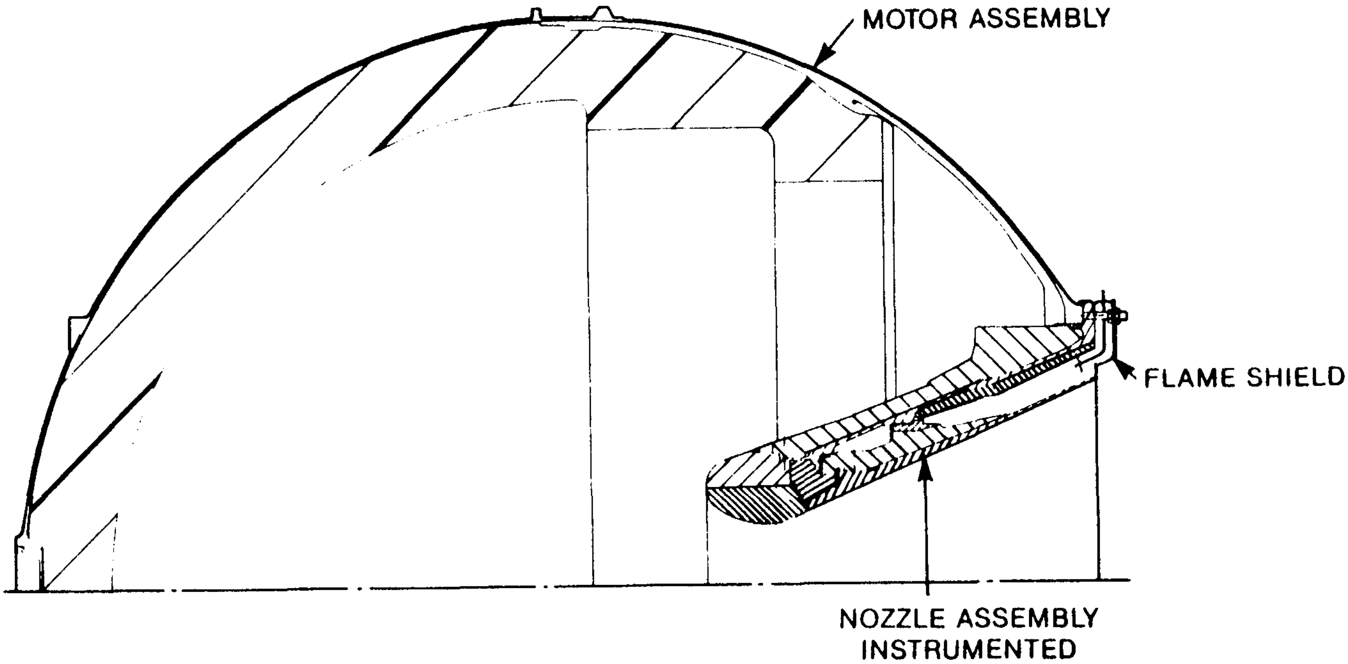


Figure 3. Motor assembly (CCT-2).

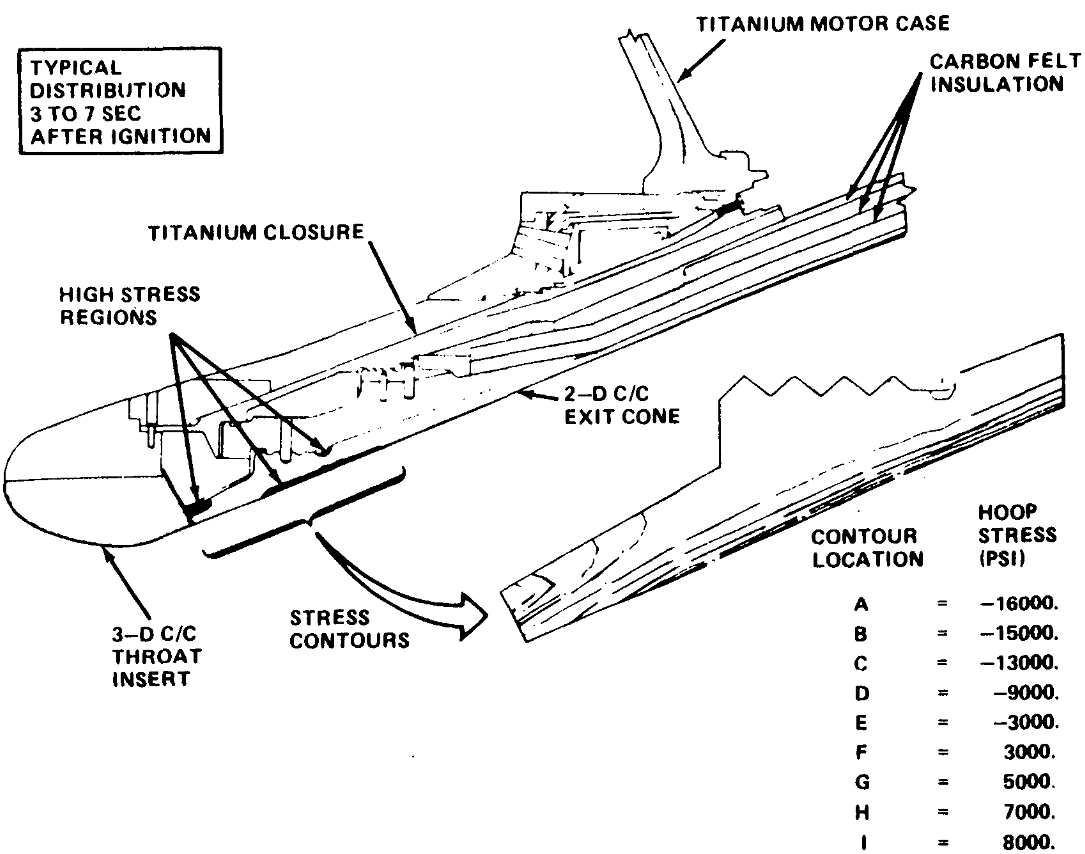


Figure 4. Areas of high stresses resulting from early thermal gradients.

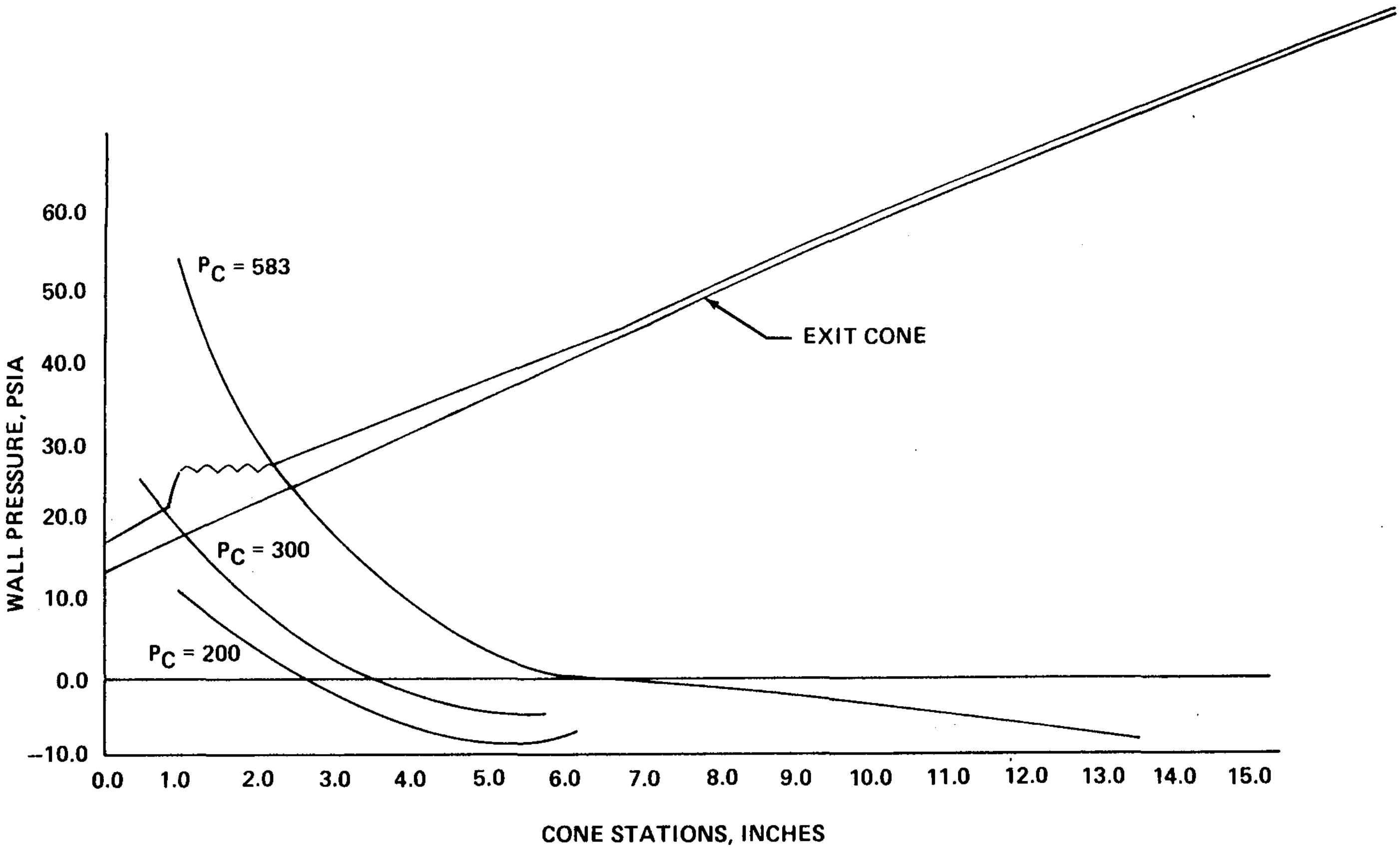


Figure 5. Internal wall pressure versus cone station.

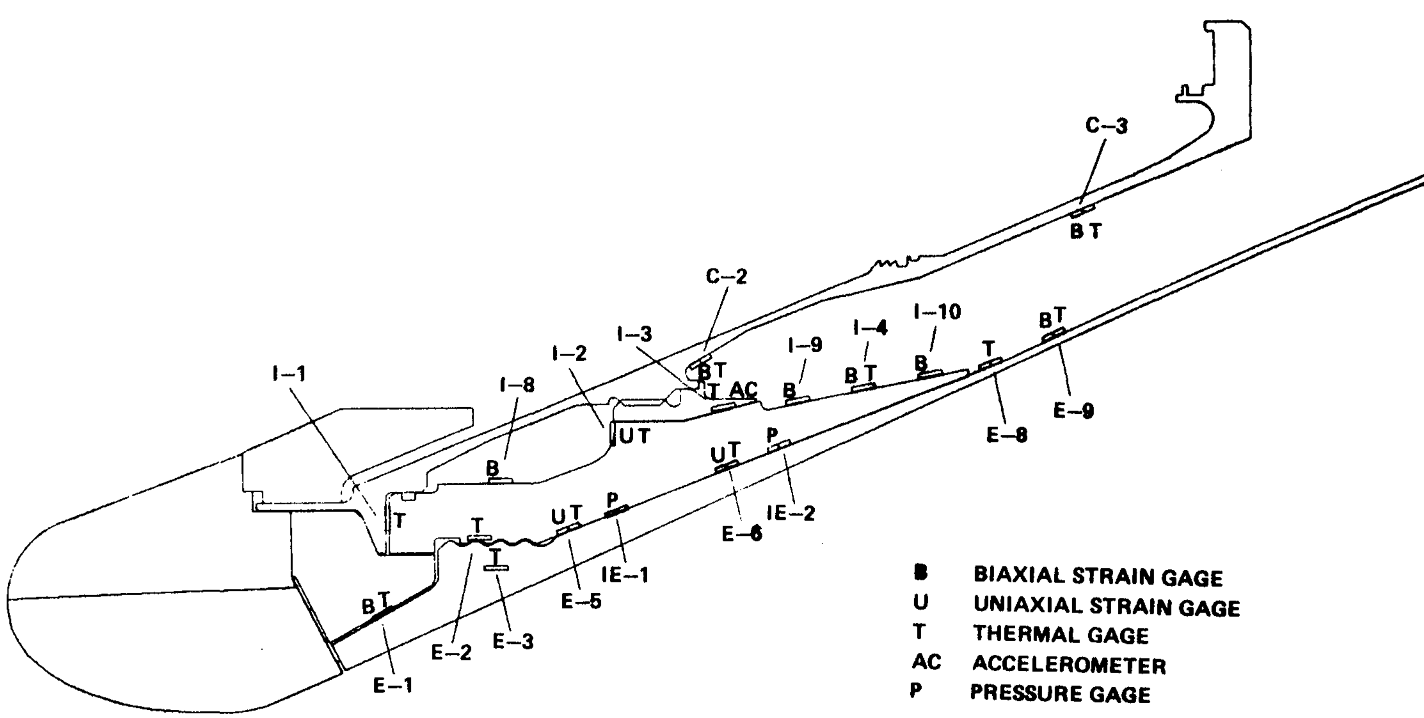


Figure 6. CCT-1 instrumentation.

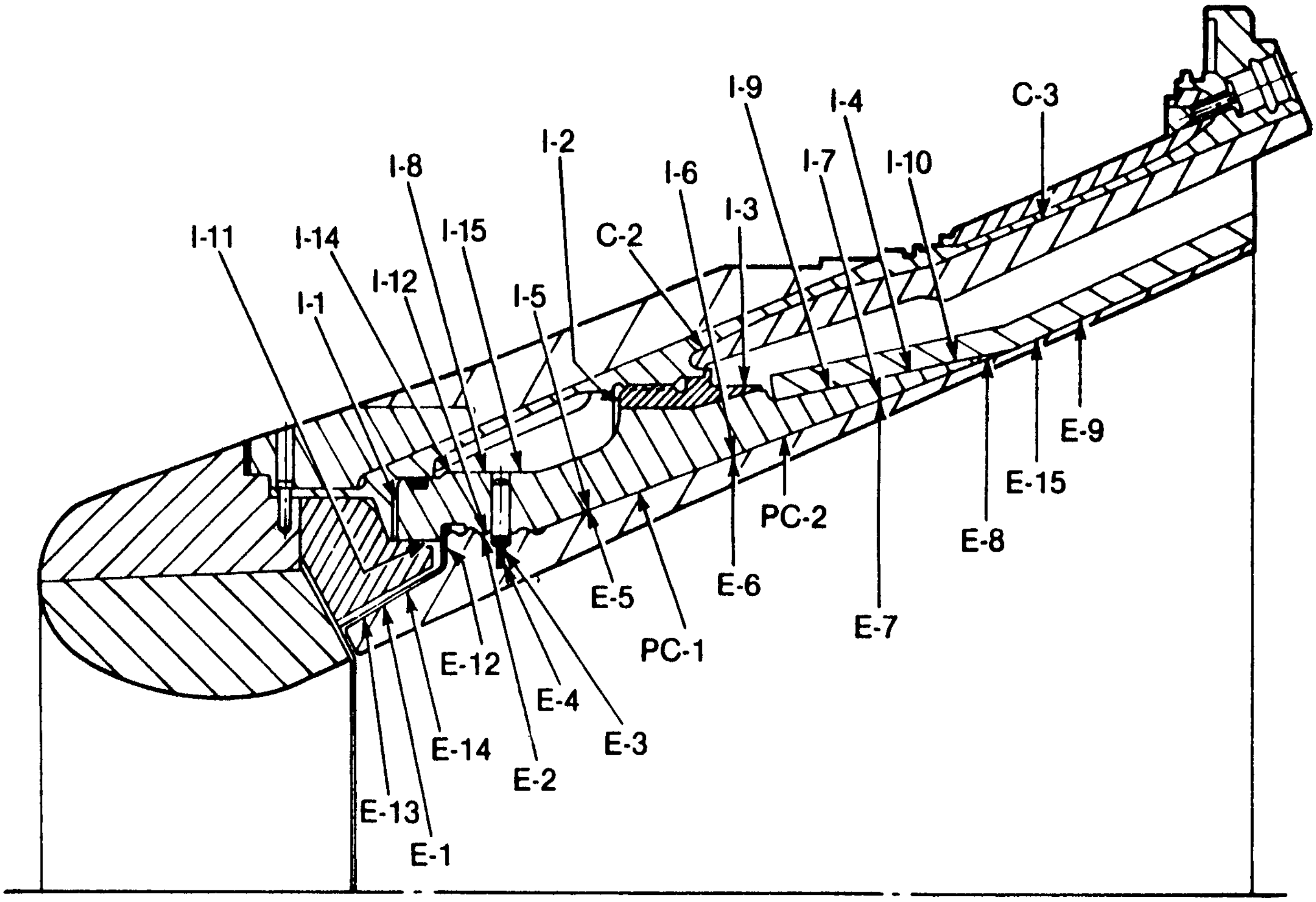


Figure 7. Instrumented nozzle assembly (CCT-2).

TABLE 1. CCT-2

| STA | A | $A^1$ | B | $B^1$ | C | $C^1$ | D | $D^1$ |
|---|---|---|---|---|---|---|---|---|
| C–1 | | | | | | | | |
| C–2 | S (H, A) T | | S (H) T | | S (H) T | | S (H) T | |
| C–3 | S (H, A) T | | T | | T | | T | |
| E–1 | S (H, A) T | | S (H, A) T | | S (H, A) T | | S (H, A) T | |
| E–2 | T | | | | T | | | |
| E–3 | T | | | | T | | | |
| E–4 | | T | | T | | T | | T |
| E–5 | T | | | | T | | | |
| E–6 | T | | | | T | | | |
| E–7 | T | | | | T | | | |
| E–8 | T | | S (H) T | | S (A) T | T | | |
| E–9 | | | S (H) | | S (A) T | | | |
| E–12 | S (H) | | S (H) | | S (H) | | S (H) | |
| E–13 | | | S (H) T | | S (A) T | | S (H) | |
| E–14 | | | S (H) T | | S (A) T | | | |
| E–15 | | | | | S (A) | | | |
| I–1 | T | | | | T | | | |
| I–2 | S (H) T | | S (H) | | S (H) T | | S (H) | |
| I–3 | T, AC | | T | | T, AC | | T | |
| I–4 | S (H, A) T | | S (H) T | | S (A) T | | T | |
| I–5 | S (H, A) T | | S (H) T | | S (H) T | | | |
| I–6 | S (H, A) T | | S (H) | | S (H) T | | | |
| I–7 | S (H, A) T | | S (H) | | S (A) T | | | |
| I–8 | S (H, A) | | S (H, A) | | S (H, A) | | S (H, A) | |
| I–9 | S (H, A) | | | | S (A) | | | |
| I–10 | S (H, A) | | | | S (A) | | | |
| I–11 | T | | | | T | | | |
| I–12 | T | | | | T | | | |
| I–14 | | | S (H) | | S (A) | | | |
| I–15 | | | S (H) | | S (A) | | | |
| PC–1 | (500) | | (500) | | (500) | | (500) | |
| PC–2 | (500) | | (500) | | (500) | | (500) | |

T = THERMOCOUPLE, S = STRAIN, (A) = AXIAL, (H) = HOOP,
PC = PRESSURE, (500) = MAX GAUGE RANGE, AC = ACCELEROMETER,
RADIAL EXCITATION

# APPENDIX A

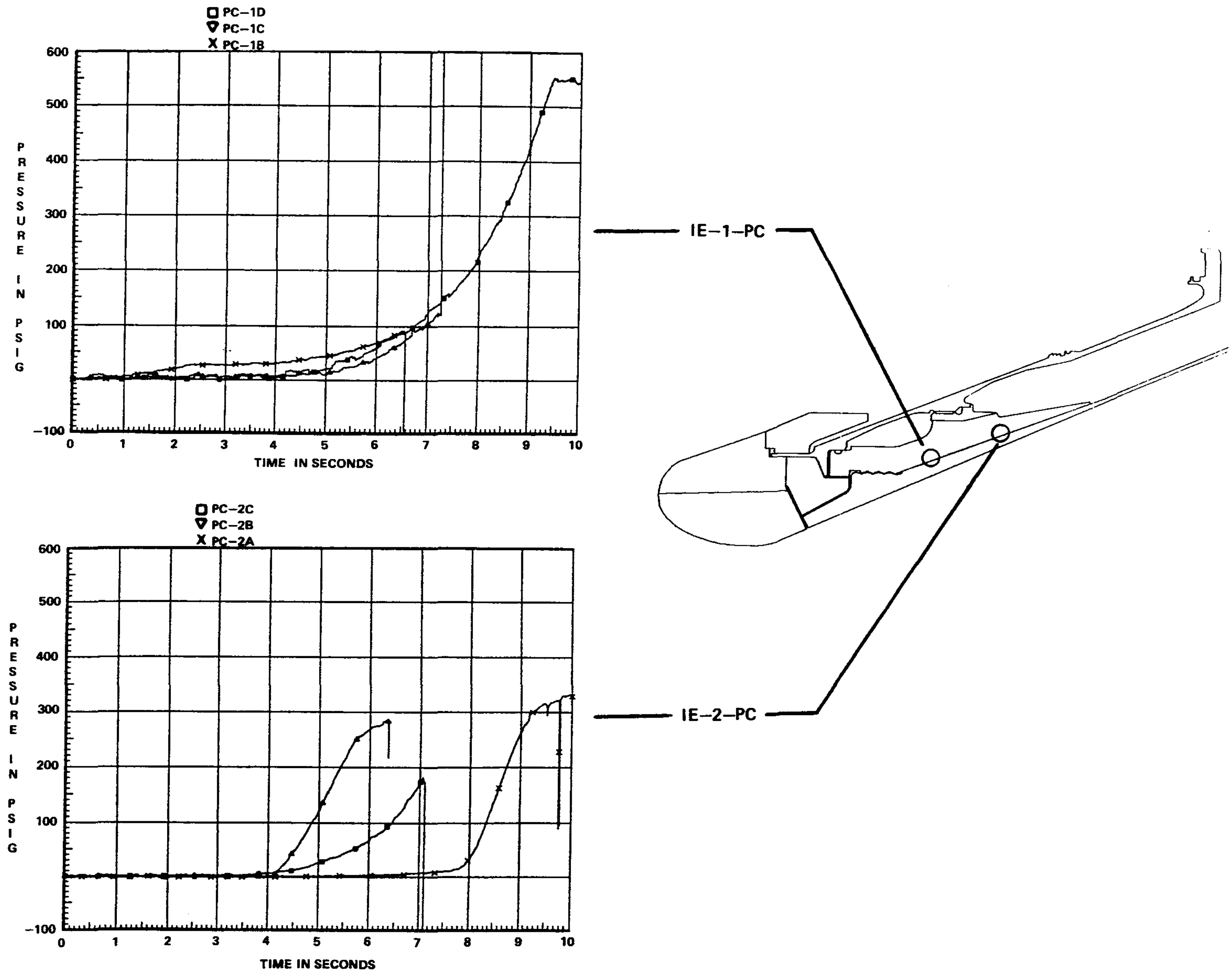

PC–1D
PC–1C
PC–1B
PRESSURE IN PSIG
TIME IN SECONDS
PC–2C
PC–2B
PC–2A
PRESSURE IN PSIG
TIME IN SECONDS
IE–1–PC
IE–2–PC


Figure A-1.

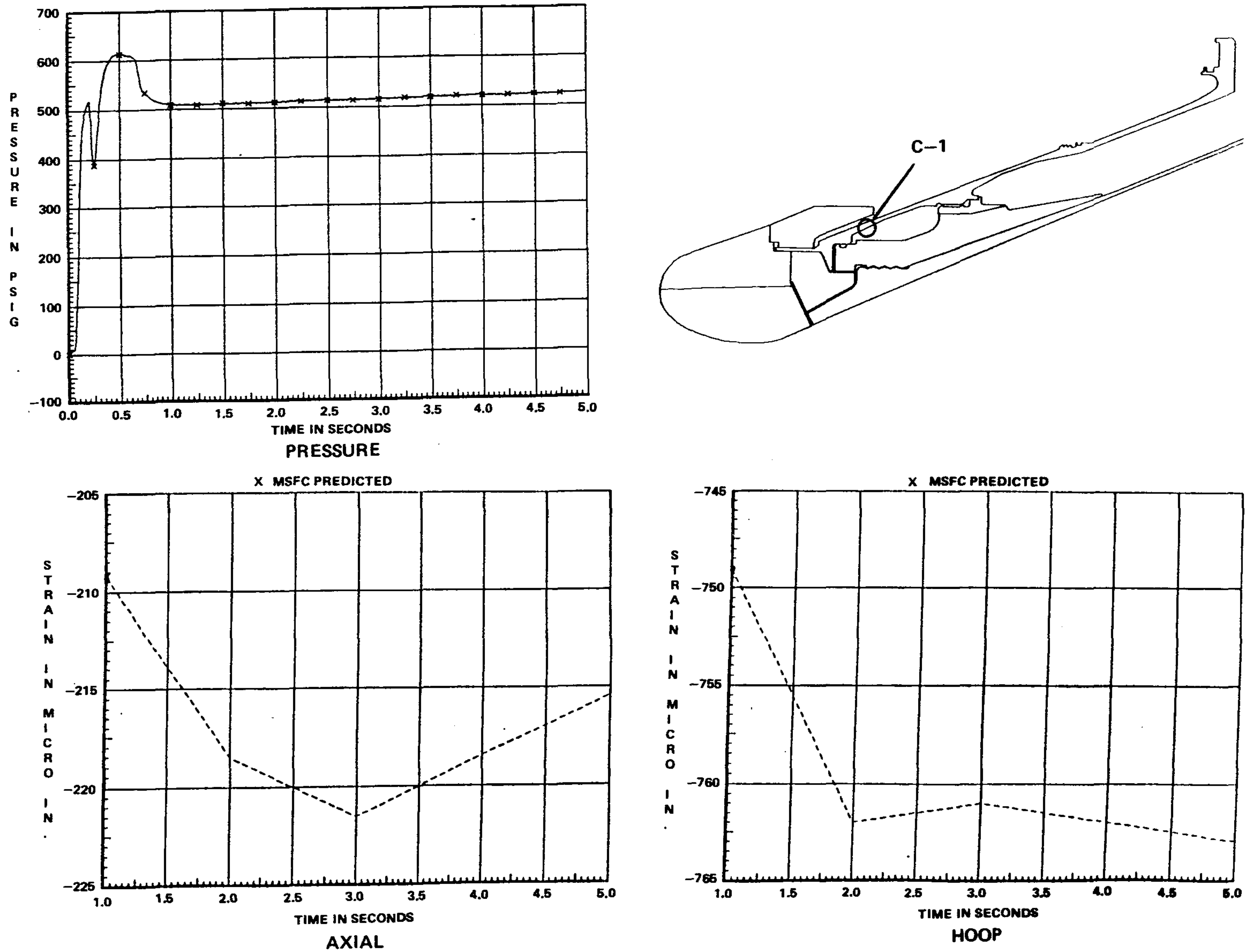

700
600
500
400
300
200
100
0
−100
PRESSURE IN PSIG
0.0
0.5
1.0
1.5
2.0
2.5
3.0
3.5
4.0
4.5
5.0
TIME IN SECONDS
PRESSURE
C–1
X MSFC PREDICTED
−205
−210
−215
−220
−225
STRAIN IN MICRO IN.
1.0
1.5
2.0
2.5
3.0
3.5
4.0
4.5
5.0
TIME IN SECONDS
AXIAL
X MSFC PREDICTED
−745
−750
−755
−760
−765
STRAIN IN MICRO IN.
1.0
1.5
2.0
2.5
3.0
3.5
4.0
4.5
5.0
TIME IN SECONDS
HOOP


Figure A-2.

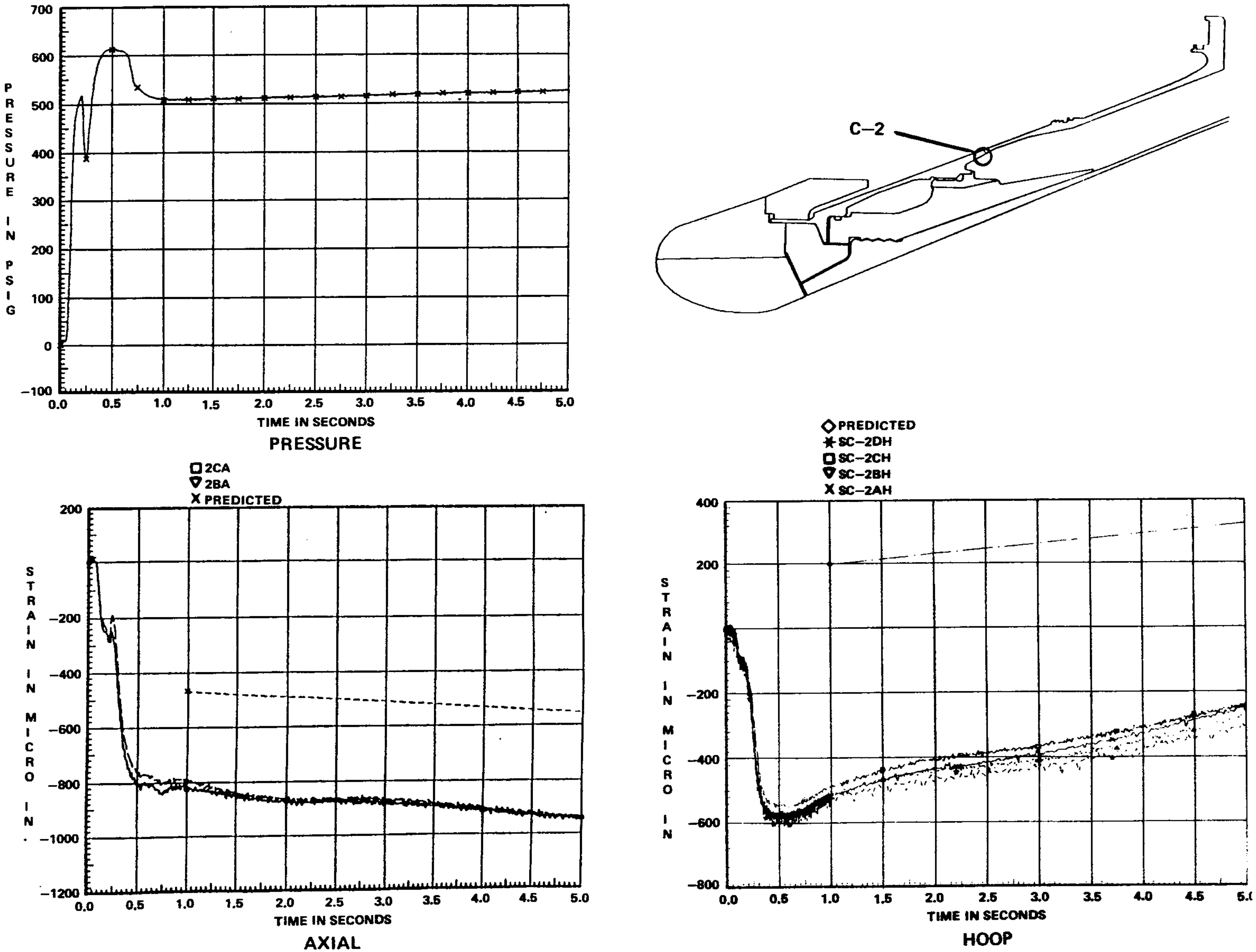
PRESSURE IN PSIG
TIME IN SECONDS
PRESSURE
C–2
2CA
2BA
X PREDICTED
STRAIN IN MICRO IN
TIME IN SECONDS
AXIAL
PREDICTED
SC–2DH
SC–2CH
SC–2BH
X SC–2AH
STRAIN IN MICRO IN
TIME IN SECONDS
HOOP

Figure A-3.

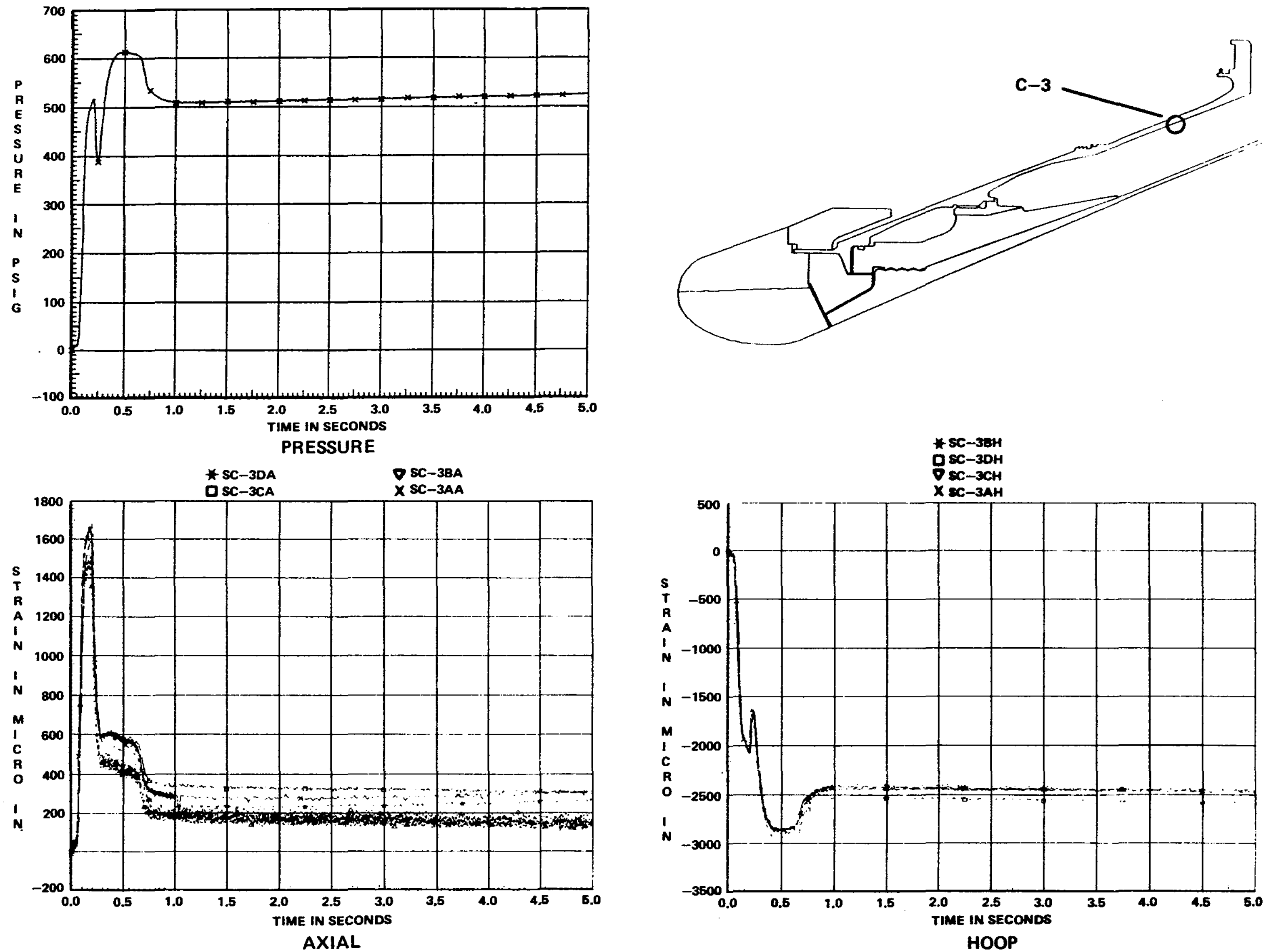
C-3
PRESSURE IN PSIG
TIME IN SECONDS
PRESSURE
SC-3DA
SC-3CA
SC-3BA
SC-3AA
STRAIN IN MICRO IN
TIME IN SECONDS
AXIAL
SC-3BH
SC-3DH
SC-3CH
SC-3AH
STRAIN IN MICRO IN
TIME IN SECONDS
HOOP

Figure A-4.

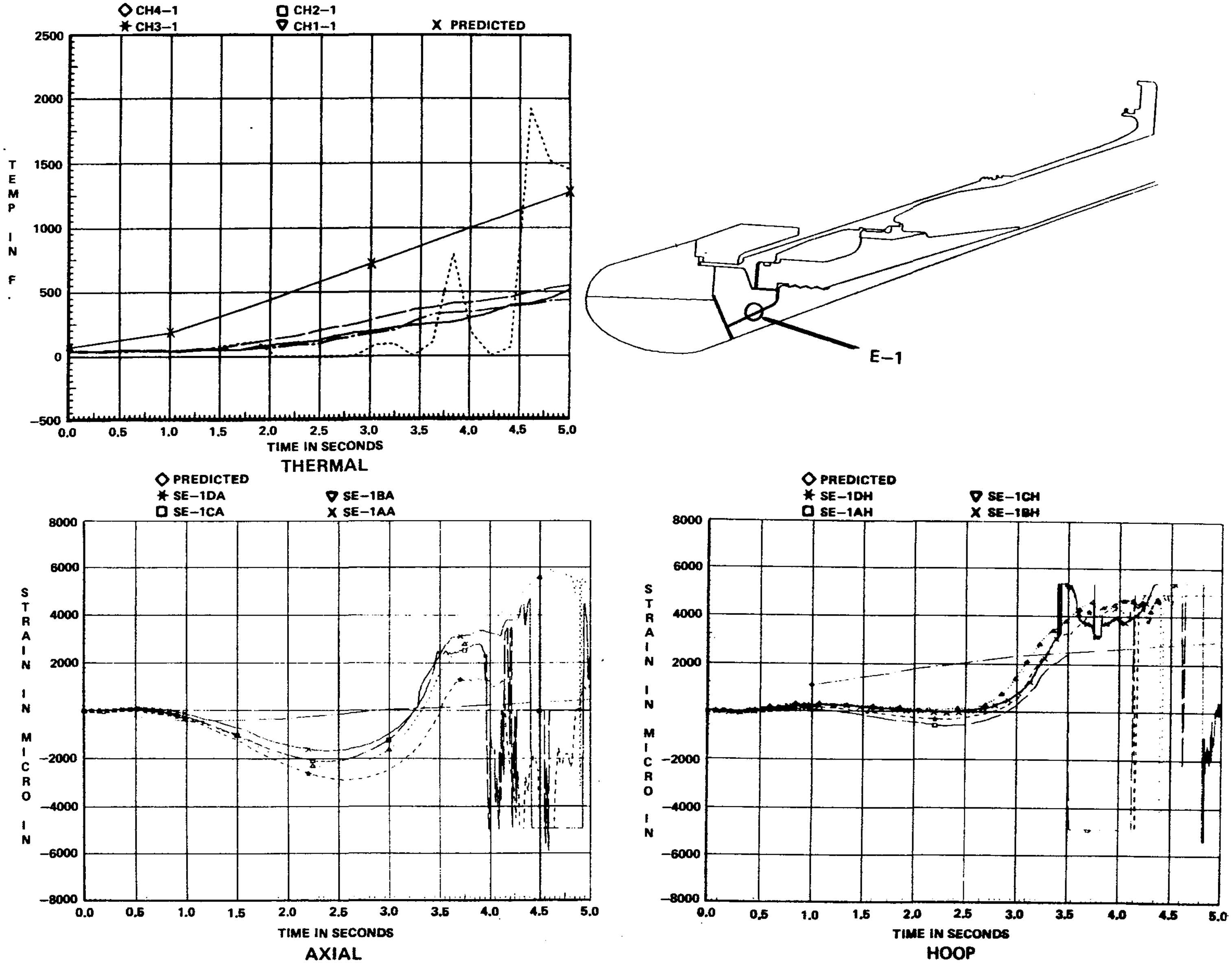
CH4–1
CH3–1
CH2–1
CH1–1
X PREDICTED
TEMP IN F.
TIME IN SECONDS
THERMAL
E–1
PREDICTED
SE–1DA
SE–1CA
SE–1BA
X SE–1AA
STRAIN IN MICRO IN
TIME IN SECONDS
AXIAL
PREDICTED
SE–1DH
SE–1AH
SE–1CH
X SE–1BH
STRAIN IN MICRO IN
TIME IN SECONDS
HOOP

Figure A-5.

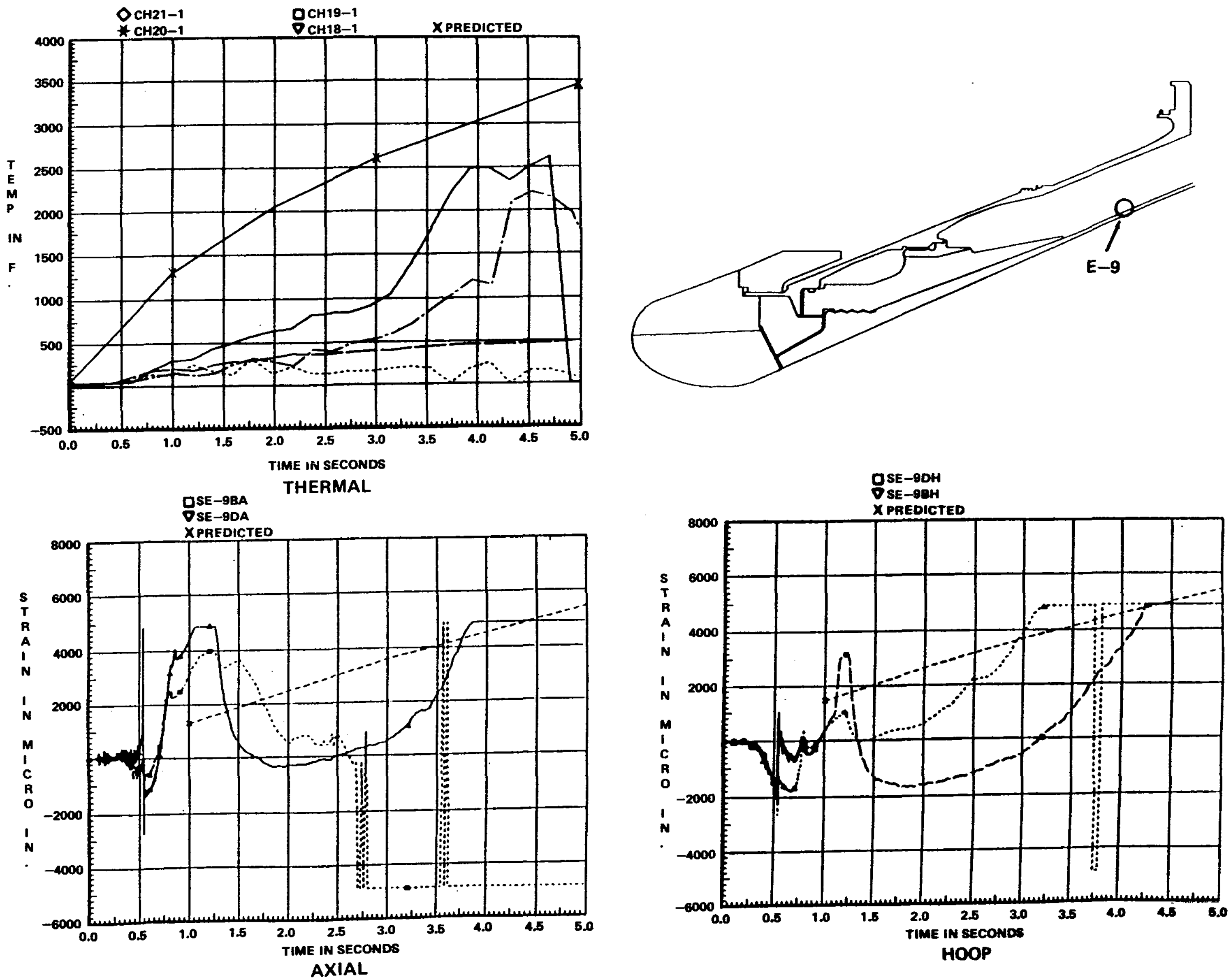
CH21–1
CH20–1
CH19–1
CH18–1
PREDICTED
TEMP IN F.
TIME IN SECONDS
THERMAL
E–9
SE–9BA
SE–9DA
PREDICTED
STRAIN IN MICRO IN.
TIME IN SECONDS
AXIAL
SE–9DH
SE–9BH
PREDICTED
STRAIN IN MICRO IN.
TIME IN SECONDS
HOOP

Figure A-6.

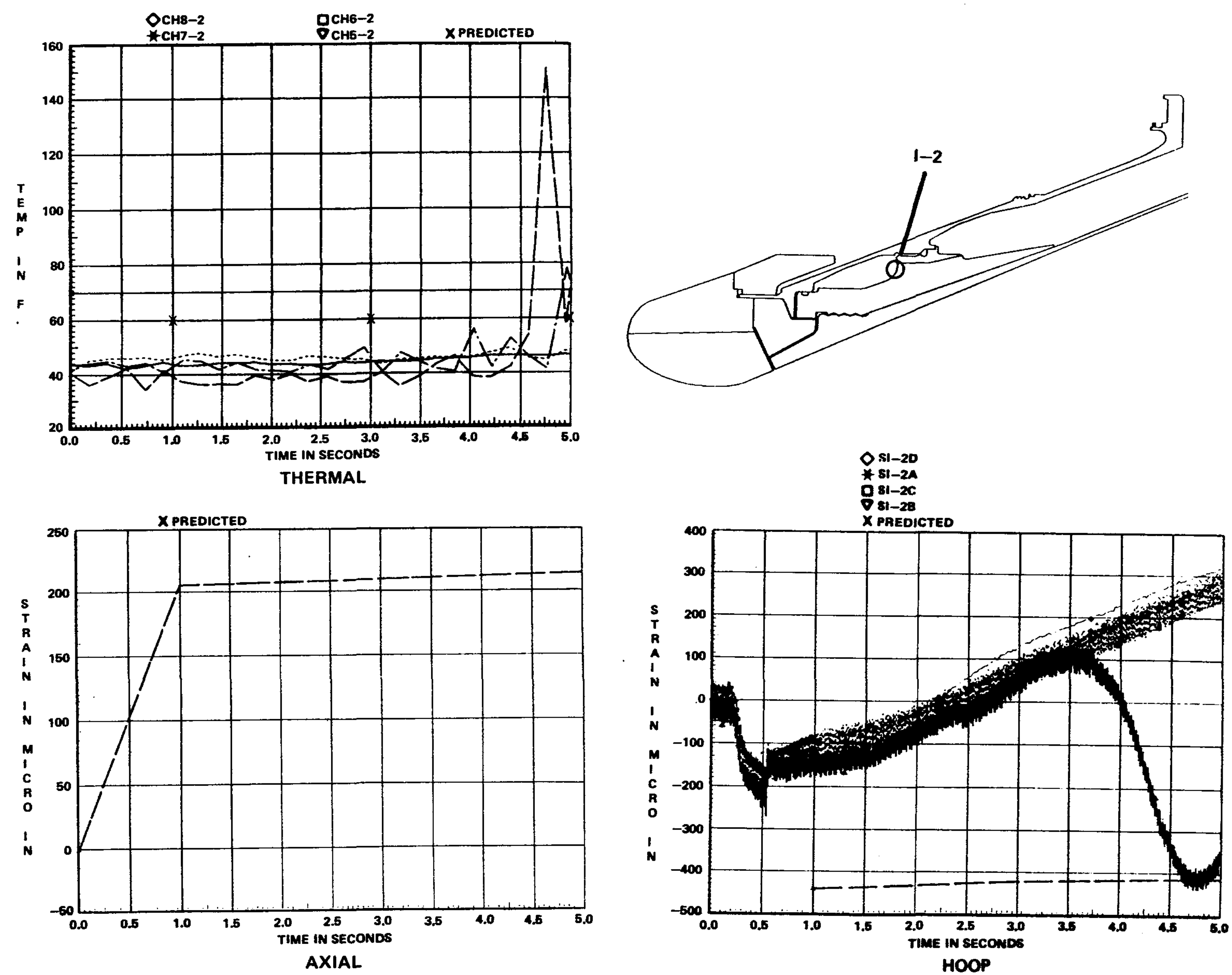

CH8-2
CH7-2
CH6-2
CH5-2
X PREDICTED
TEMP IN F.
TIME IN SECONDS
THERMAL
I-2
X PREDICTED
STRAIN IN MICRO IN
TIME IN SECONDS
AXIAL
SI-2D
SI-2A
SI-2C
SI-2B
X PREDICTED
STRAIN IN MICRO IN
TIME IN SECONDS
HOOP


Figure A-7.

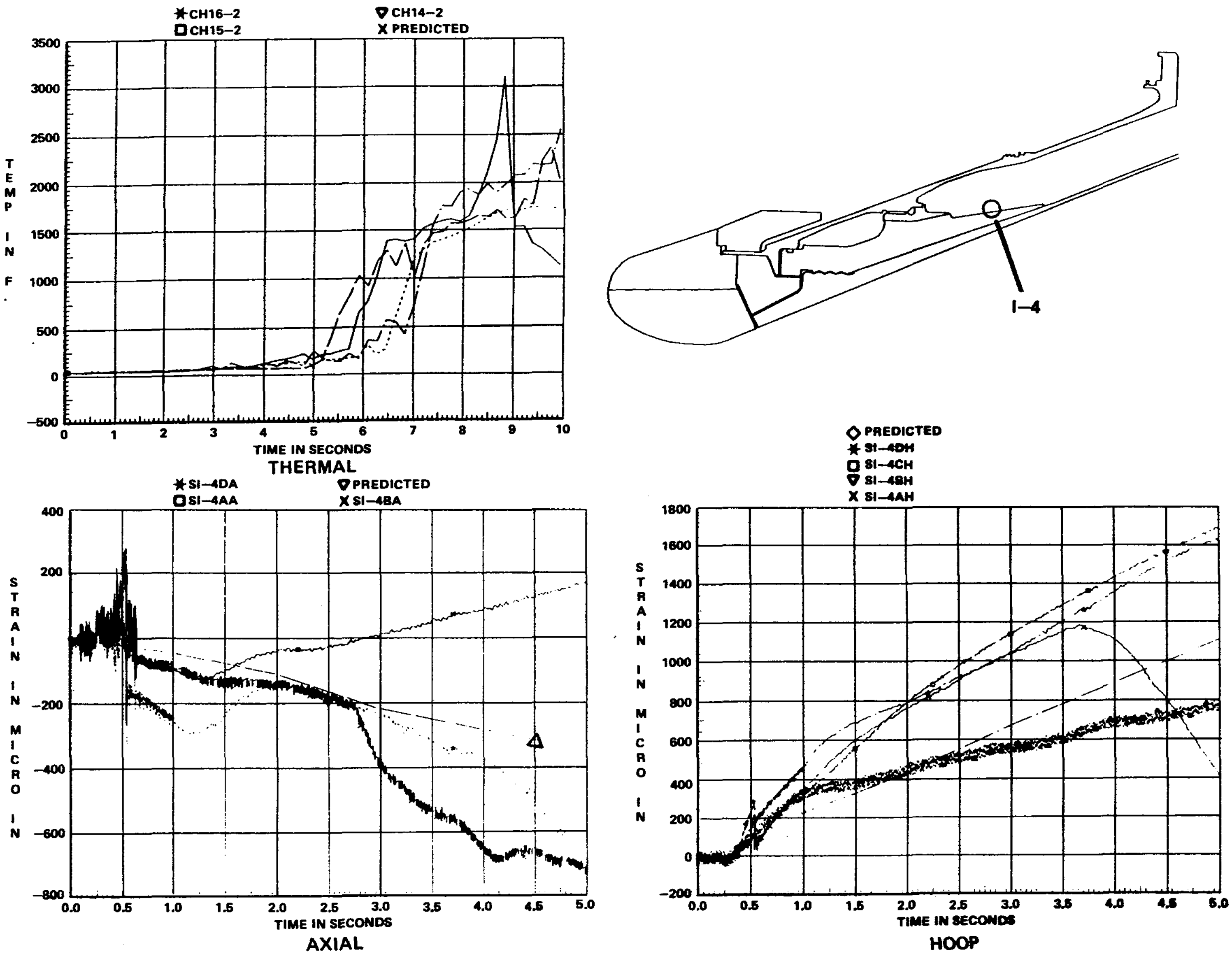
CH16–2
CH15–2
CH14–2
PREDICTED
TEMP IN F.
TIME IN SECONDS
THERMAL
I–4
SI–4DA
SI–4AA
PREDICTED
SI–4BA
STRAIN IN MICRO IN
TIME IN SECONDS
AXIAL
PREDICTED
SI–4DH
SI–4CH
SI–4BH
SI–4AH
STRAIN IN MICRO IN
TIME IN SECONDS
HOOP

Figure A-8.

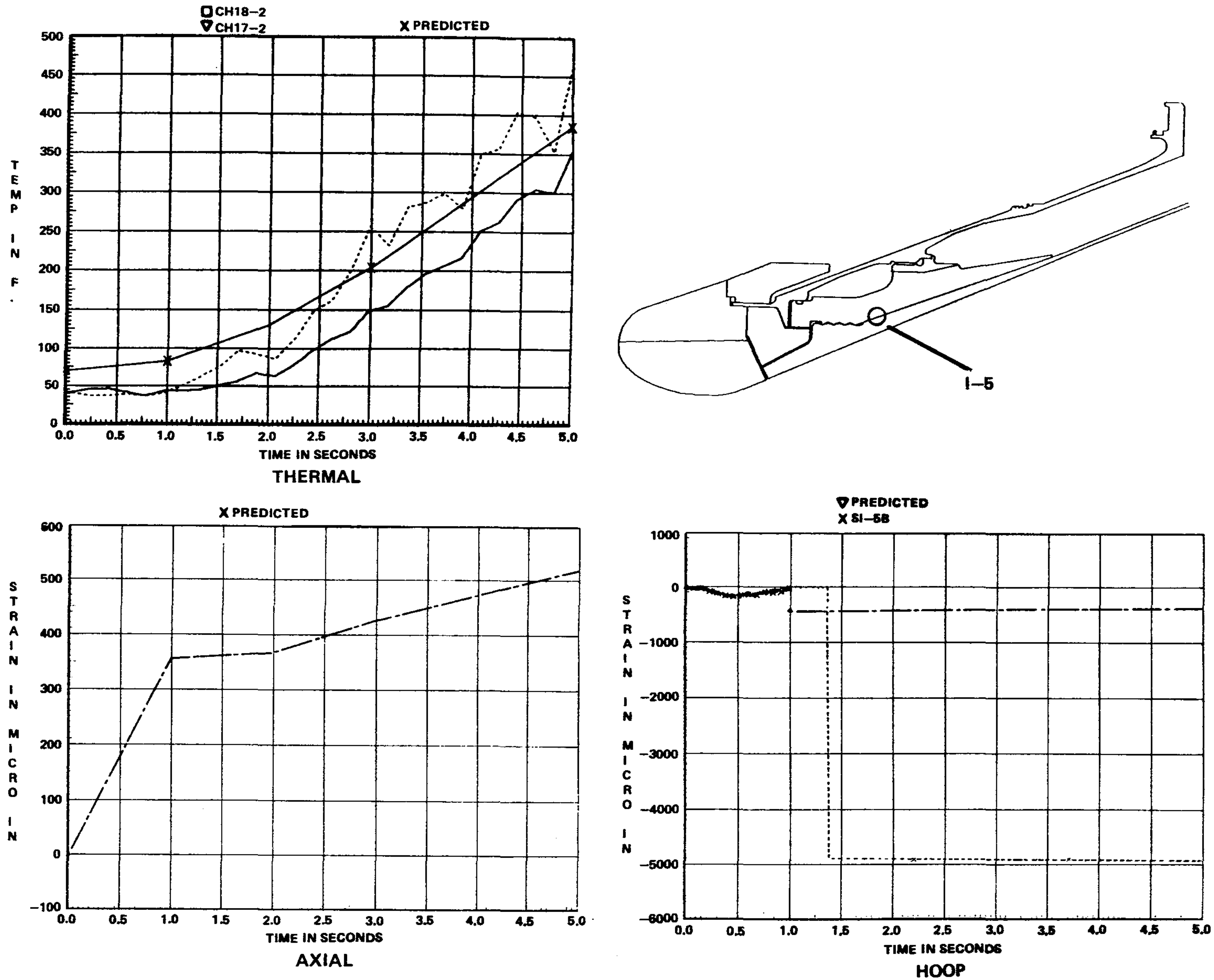

CH18–2
CH17–2
X PREDICTED
TEMP IN F.
TIME IN SECONDS
THERMAL
I–5
X PREDICTED
STRAIN IN MICRO IN
TIME IN SECONDS
AXIAL
PREDICTED
X SI–5B
STRAIN IN MICRO IN
TIME IN SECONDS
HOOP


Figure A-9.

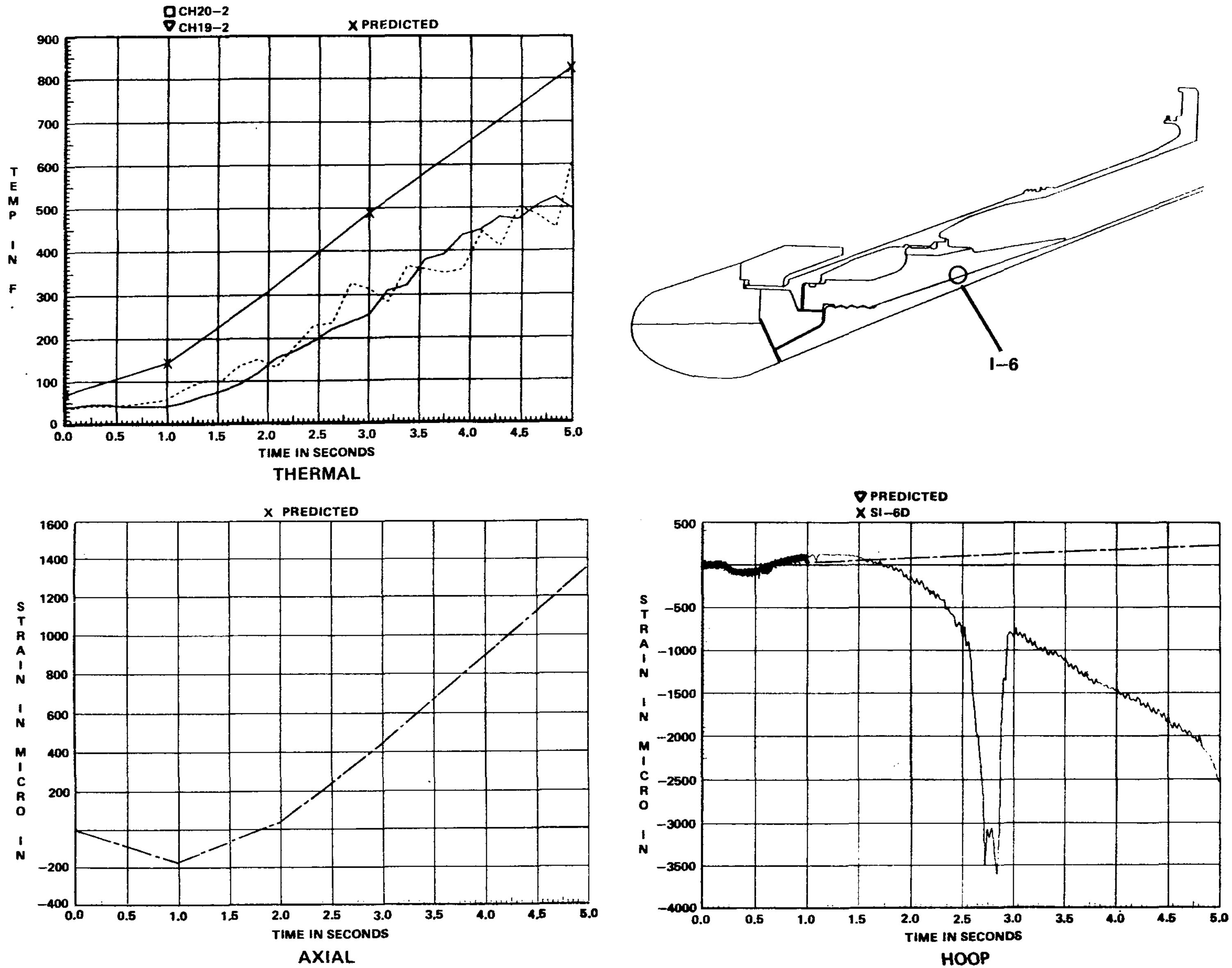
CH20–2
CH19–2
X PREDICTED
TEMP IN F.
TIME IN SECONDS
THERMAL
I–6
X PREDICTED
STRAIN IN MICRO IN
TIME IN SECONDS
AXIAL
PREDICTED
X SI–6D
STRAIN IN MICRO IN
TIME IN SECONDS
HOOP

Figure A-10.

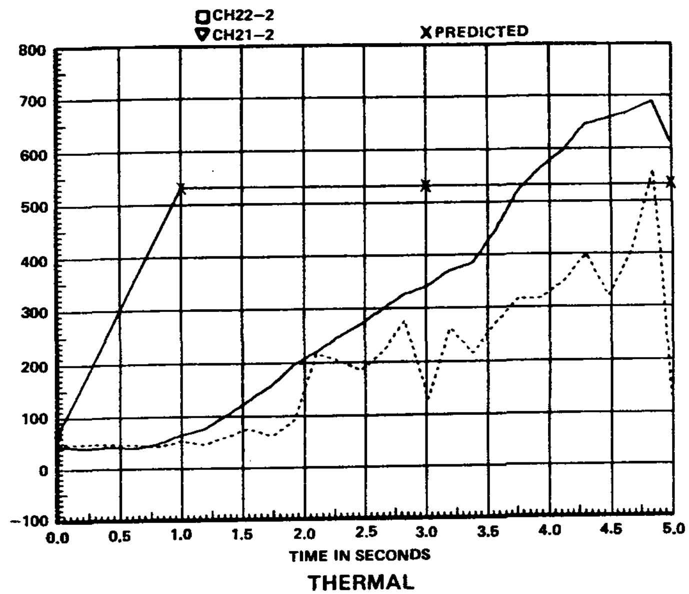
CH22-2
CH21-2
X PREDICTED
TEMP IN F.
800
700
600
500
400
300
200
100
0
-100
0.0
0.5
1.0
1.5
2.0
2.5
3.0
3.5
4.0
4.5
5.0
TIME IN SECONDS
THERMAL

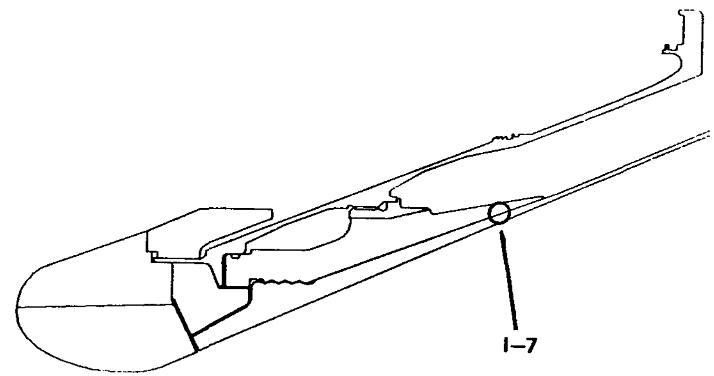
I-7

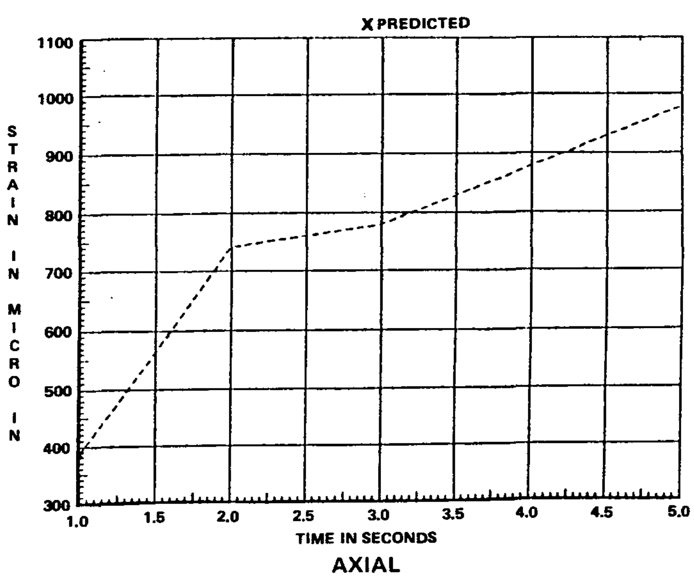
X PREDICTED
STRAIN IN MICRO IN
1100
1000
900
800
700
600
500
400
300
1.0
1.5
2.0
2.5
3.0
3.5
4.0
4.5
5.0
TIME IN SECONDS
AXIAL

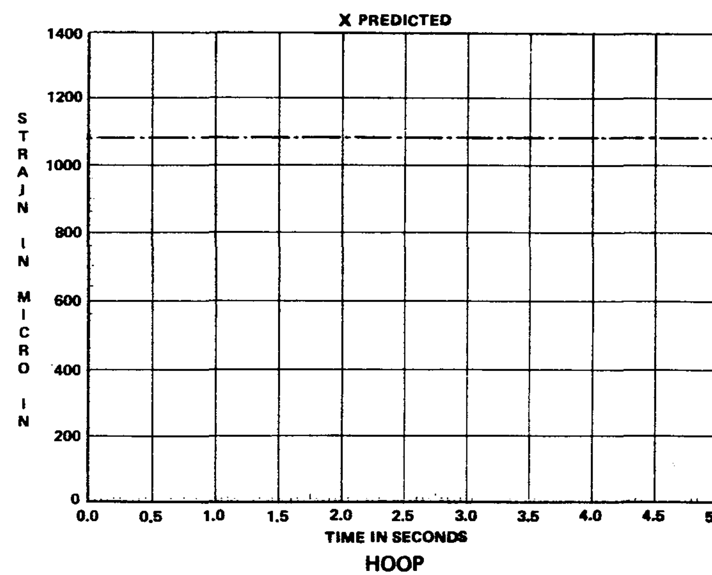
X PREDICTED
STRAIN IN MICRO IN
1400
1200
1000
800
600
400
200
0
0.0
0.5
1.0
1.5
2.0
2.5
3.0
3.5
4.0
4.5
5.0
TIME IN SECONDS
HOOP

Figure A-11.

THERMAL DATA
NOT RECORDED

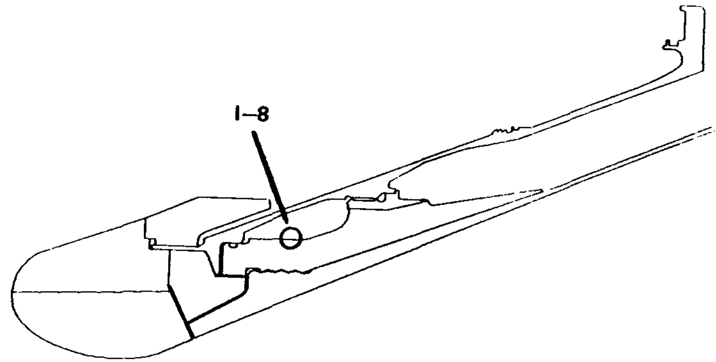


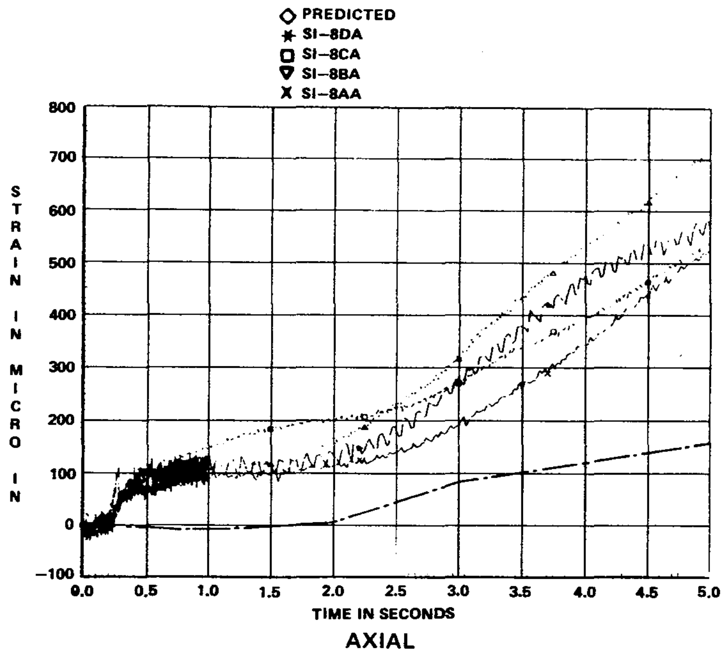


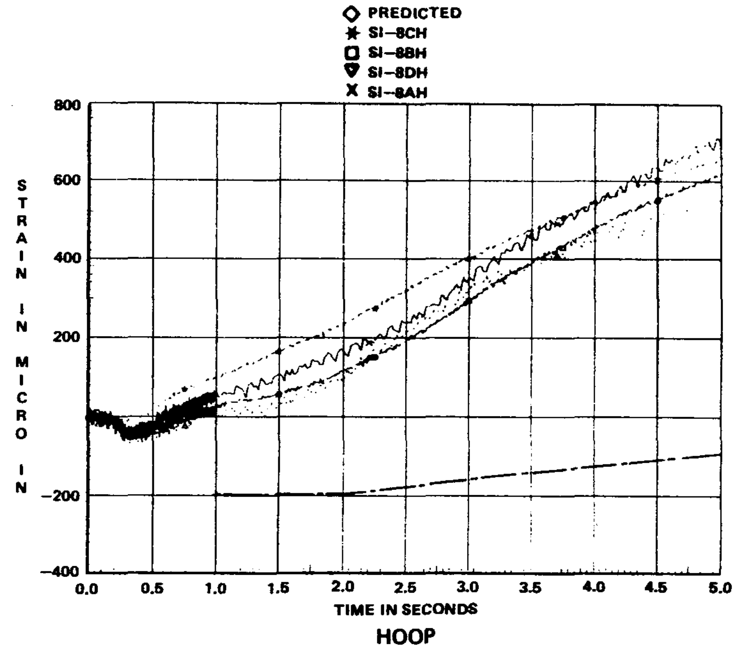


Figure A-12.

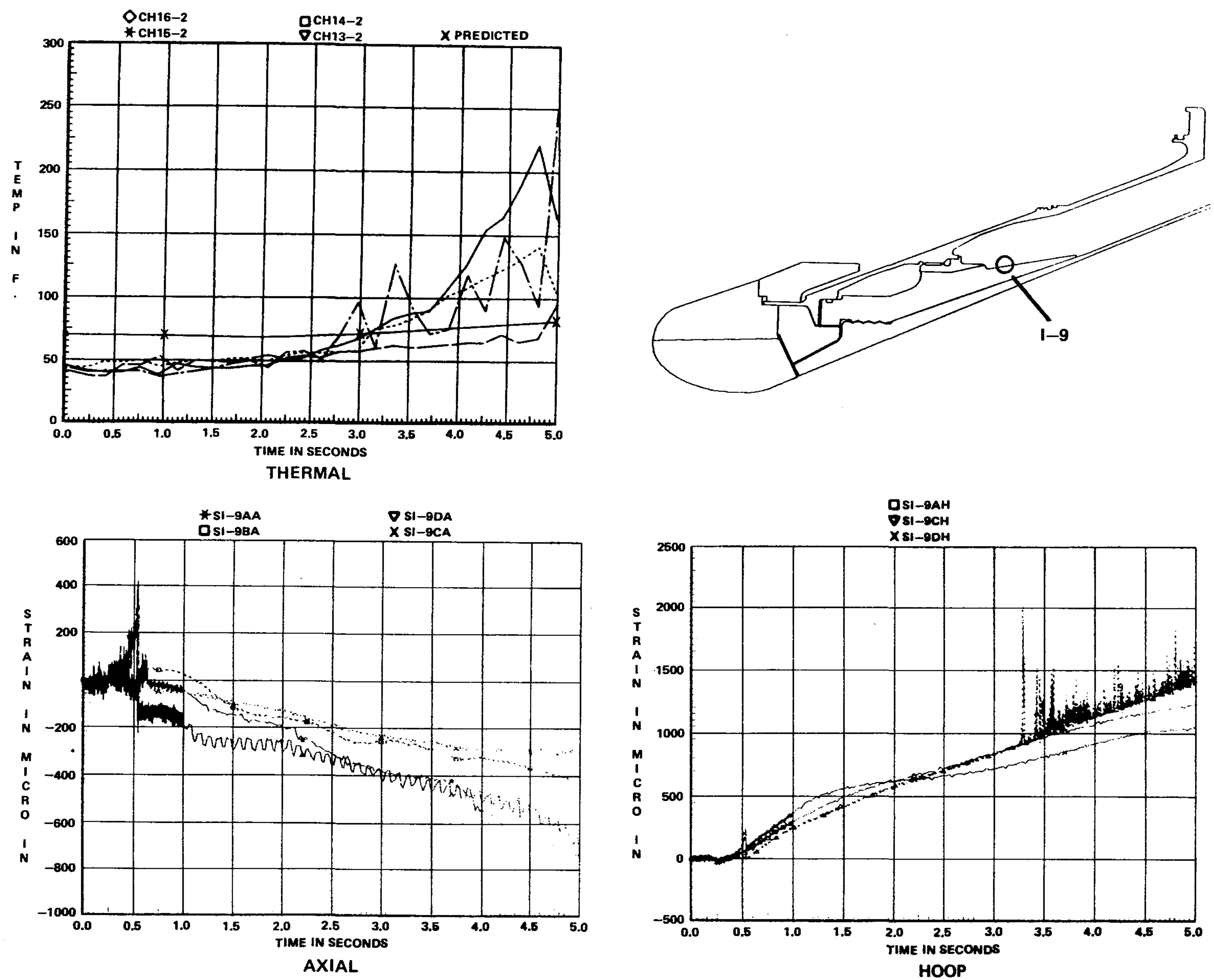
CH16–2
CH15–2
CH14–2
CH13–2
X PREDICTED
TEMP IN F.
TIME IN SECONDS
THERMAL
I–9
SI–9AA
SI–9BA
SI–9DA
SI–9CA
STRAIN IN MICRO IN
TIME IN SECONDS
AXIAL
SI–9AH
SI–9CH
SI–9DH
STRAIN IN MICRO IN
TIME IN SECONDS
HOOP

Figure A-13.

THERMAL DATA
NOT RECORDED

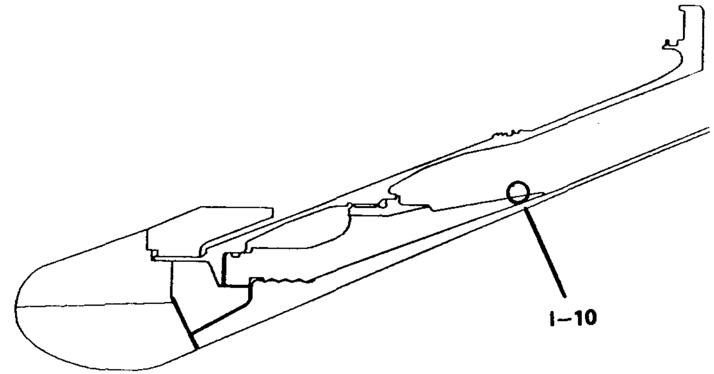


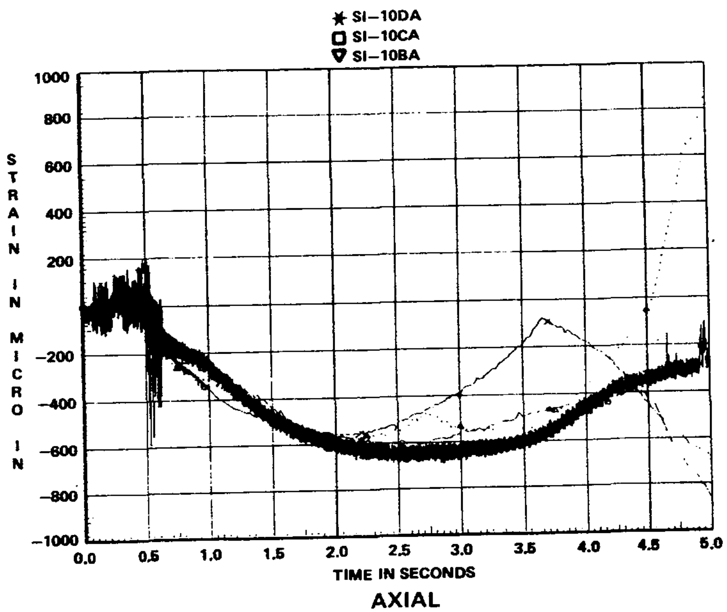


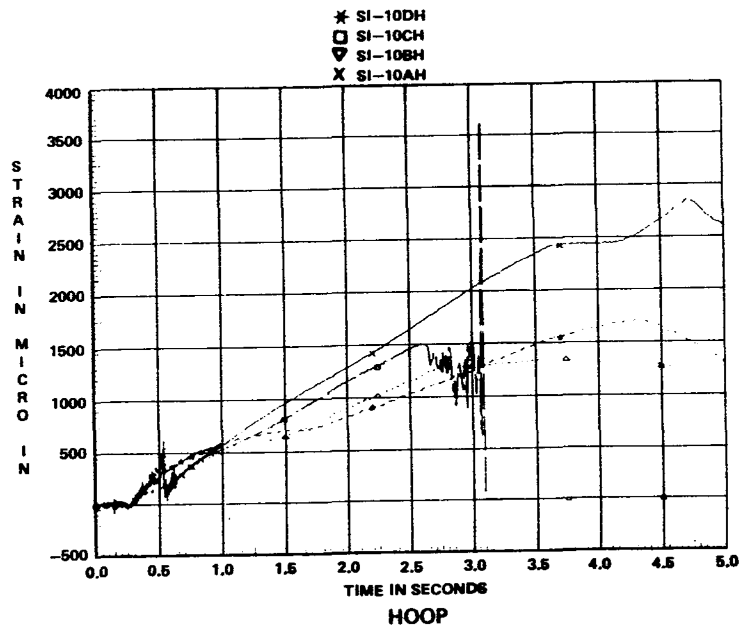


Figure A-14.

# APPENDIX B

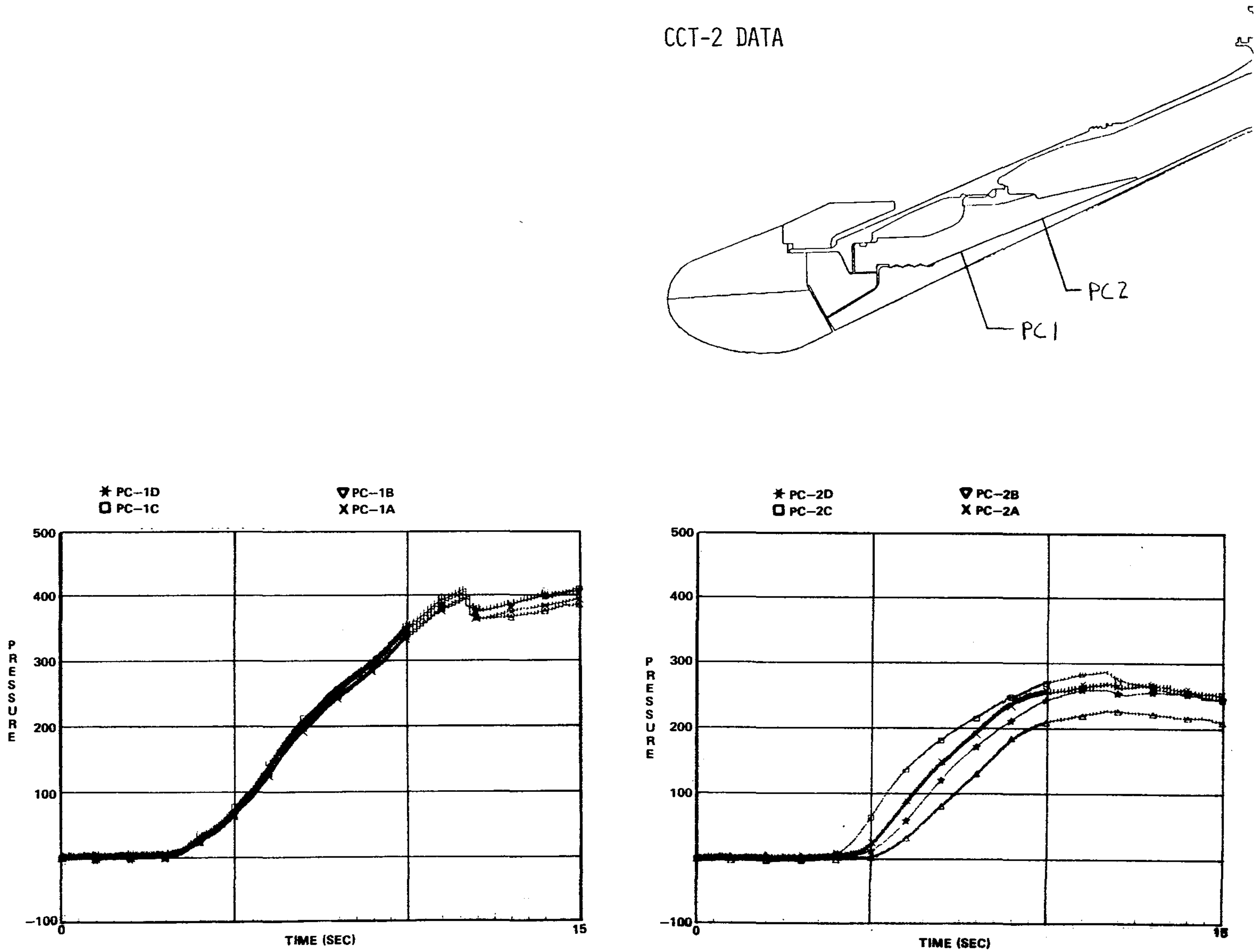
CCT-2 DATA
PC2
PC1
PC-1D
PC-1C
PC-1B
PC-1A
500
400
300
200
100
-100
0
15
PRESSURE
TIME (SEC)
PC-2D
PC-2C
PC-2B
PC-2A
500
400
300
200
100
-100
0
15
PRESSURE
TIME (SEC)

Figure B-1.

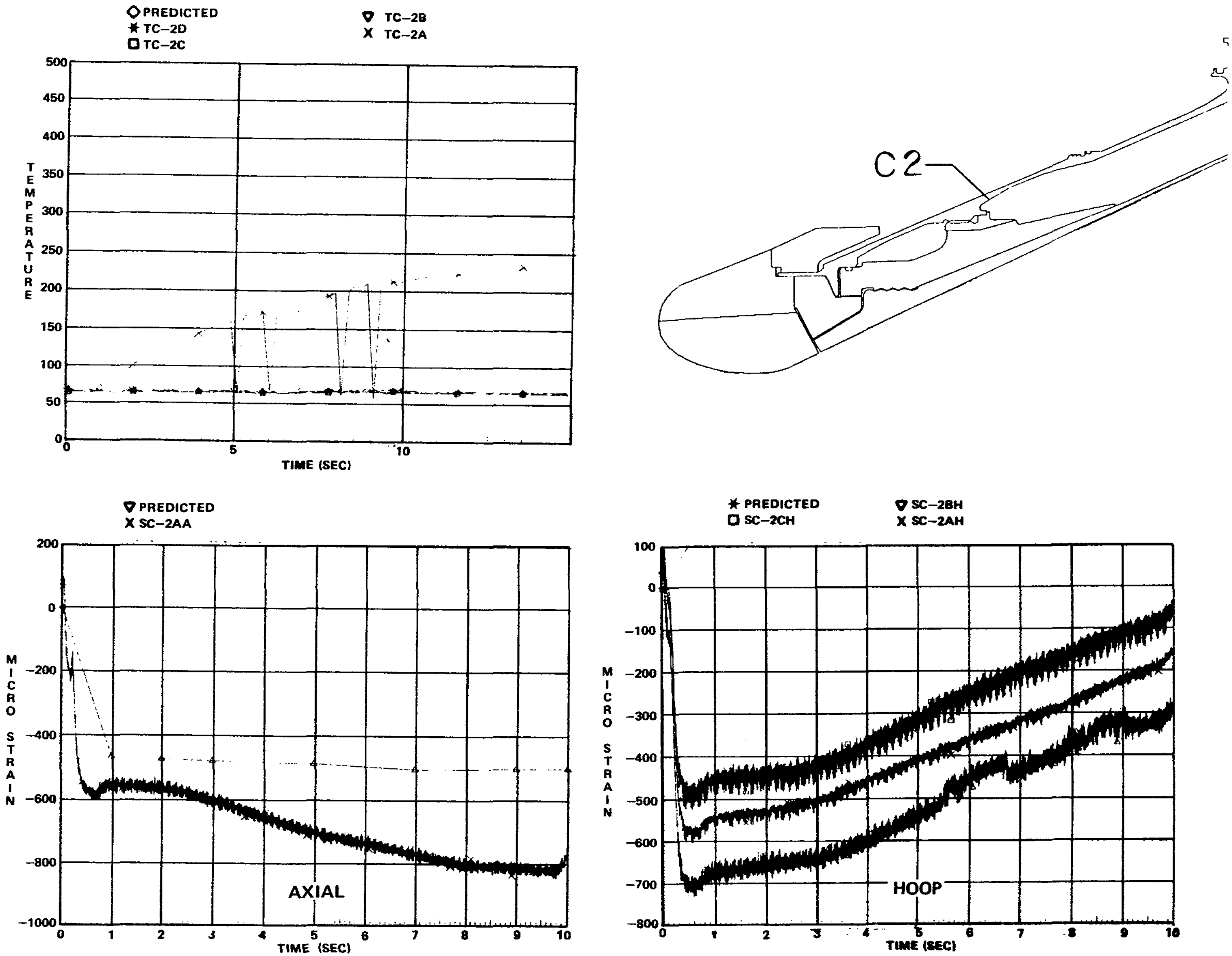
◇ PREDICTED
✱ TC–2D
□ TC–2C
▽ TC–2B
X TC–2A
TEMPERATURE
TIME (SEC)
C2
▽ PREDICTED
X SC–2AA
MICRO STRAIN
AXIAL
TIME (SEC)
✱ PREDICTED
□ SC–2CH
▽ SC–2BH
X SC–2AH
MICRO STRAIN
HOOP
TIME (SEC)

Figure B-2.

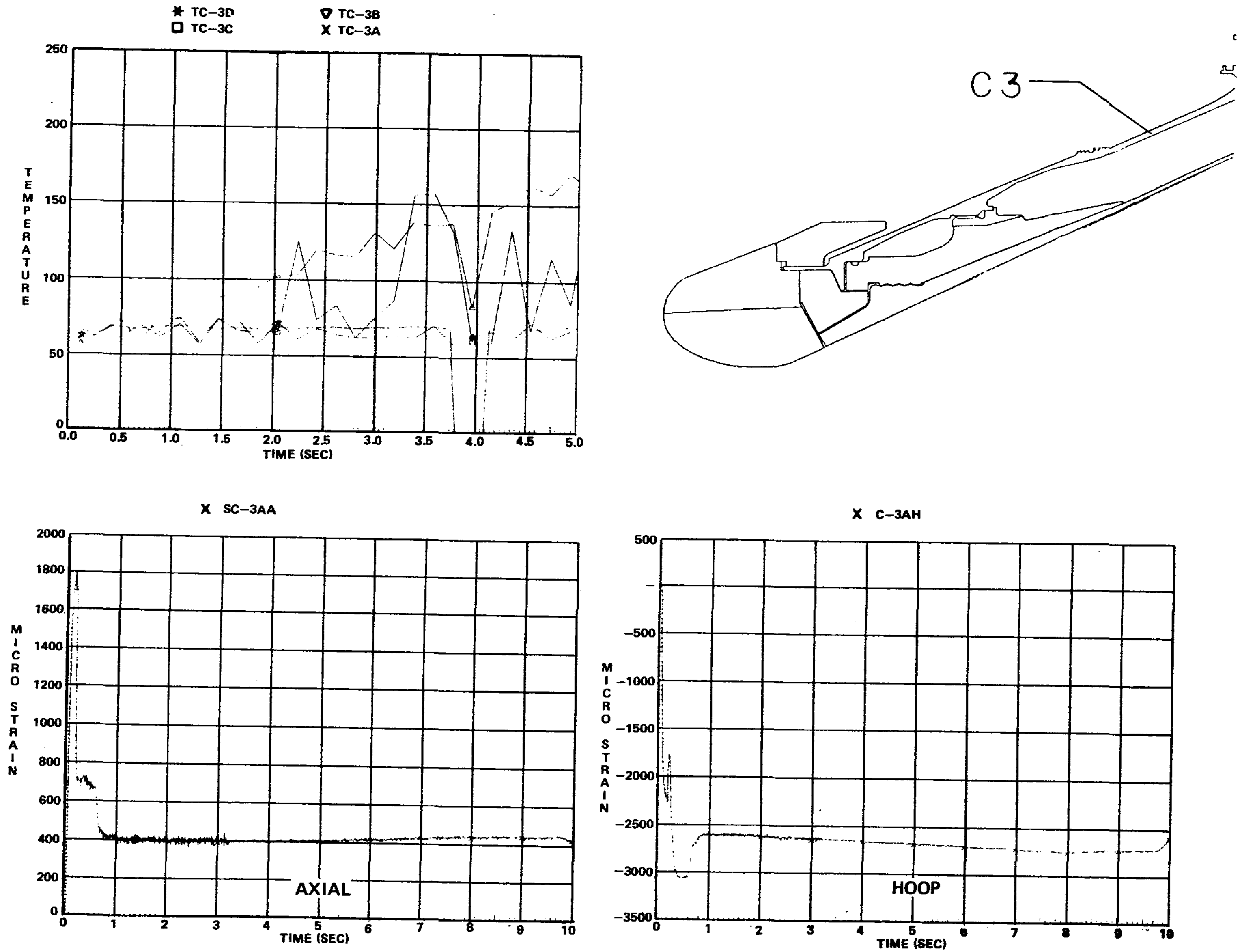

TC-3D
TC-3C
TC-3B
TC-3A
TEMPERATURE
250
200
150
100
50
0
0.0 0.5 1.0 1.5 2.0 2.5 3.0 3.5 4.0 4.5 5.0
TIME (SEC)
C3
X SC-3AA
MICRO STRAIN
2000
1800
1600
1400
1200
1000
800
600
400
200
0
AXIAL
0 1 2 3 4 5 6 7 8 9 10
TIME (SEC)
X C-3AH
MICRO STRAIN
500
-500
-1000
-1500
-2000
-2500
-3000
-3500
HOOP
0 1 2 3 4 5 6 7 8 9 10
TIME (SEC)


Figure B-3.

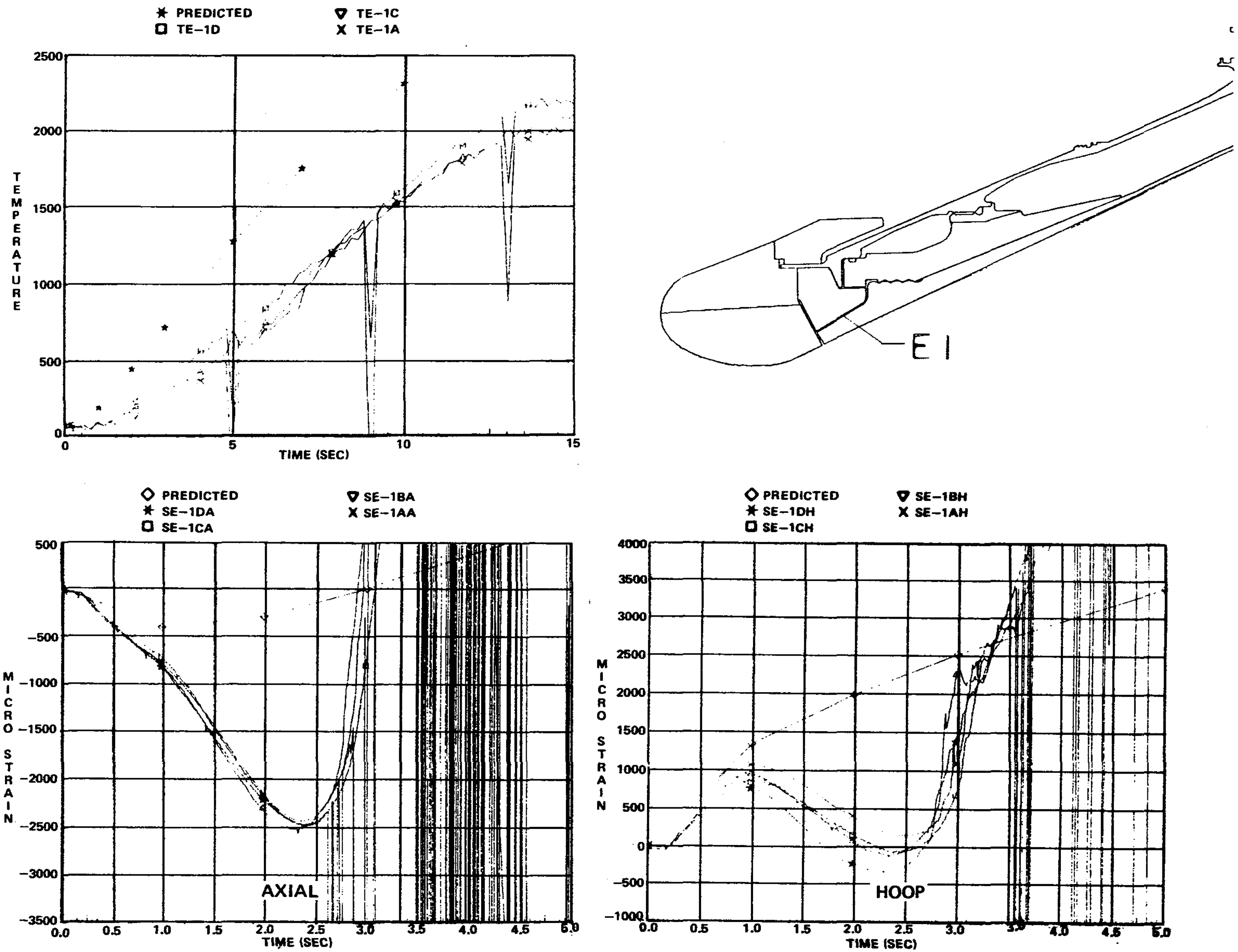

PREDICTED
TE-1D
TE-1C
TE-1A
TEMPERATURE
TIME (SEC)
E1
PREDICTED
SE-1DA
SE-1CA
SE-1BA
SE-1AA
MICRO STRAIN
AXIAL
TIME (SEC)
PREDICTED
SE-1DH
SE-1CH
SE-1BH
SE-1AH
MICRO STRAIN
HOOP
TIME (SEC)


Figure B-4.

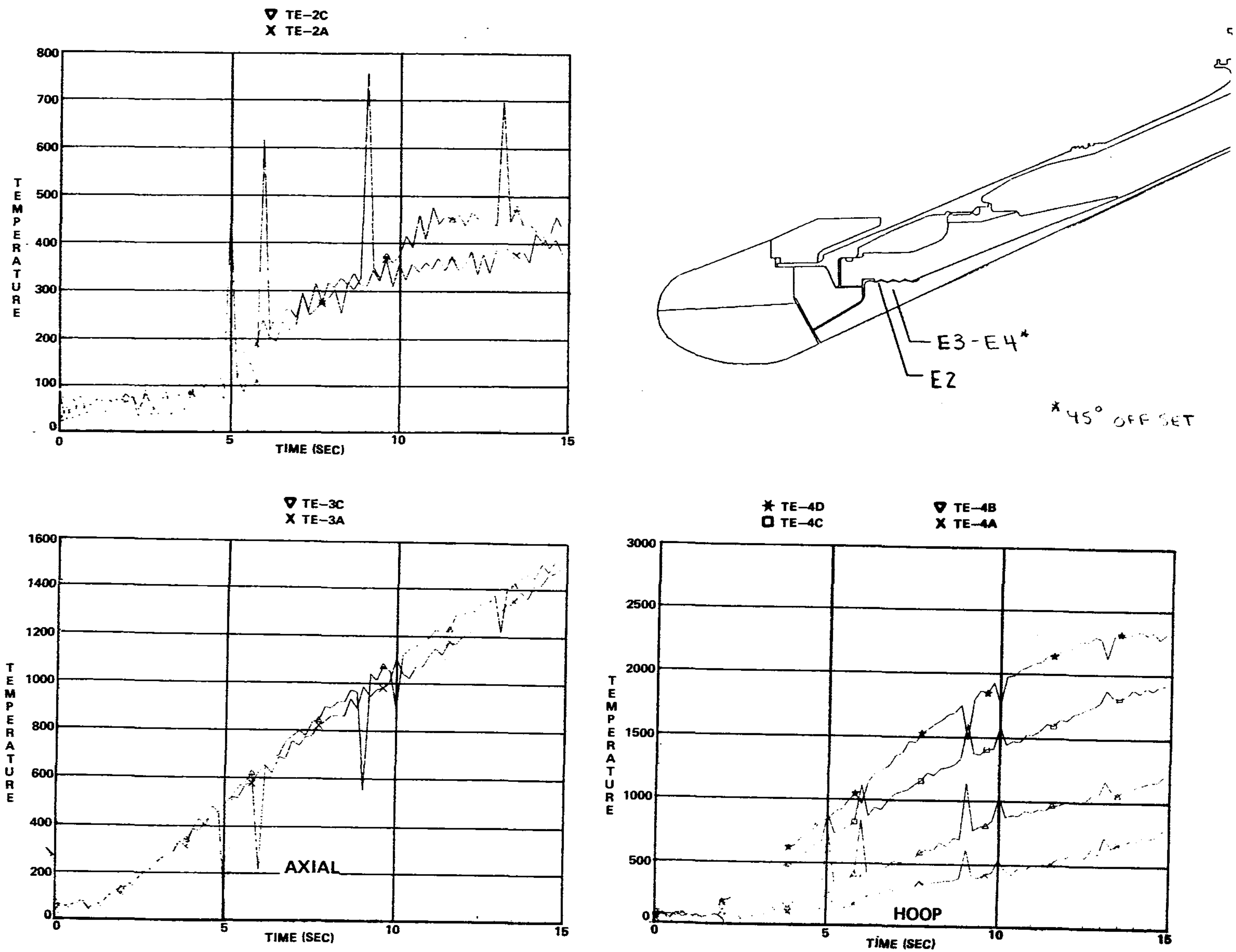
TE-2C
TE-2A
TEMPERATURE
TIME (SEC)
E3-E4*
E2
*45° OFF SET
TE-3C
TE-3A
AXIAL
TE-4D
TE-4C
TE-4B
TE-4A
HOOP

Figure B-5.

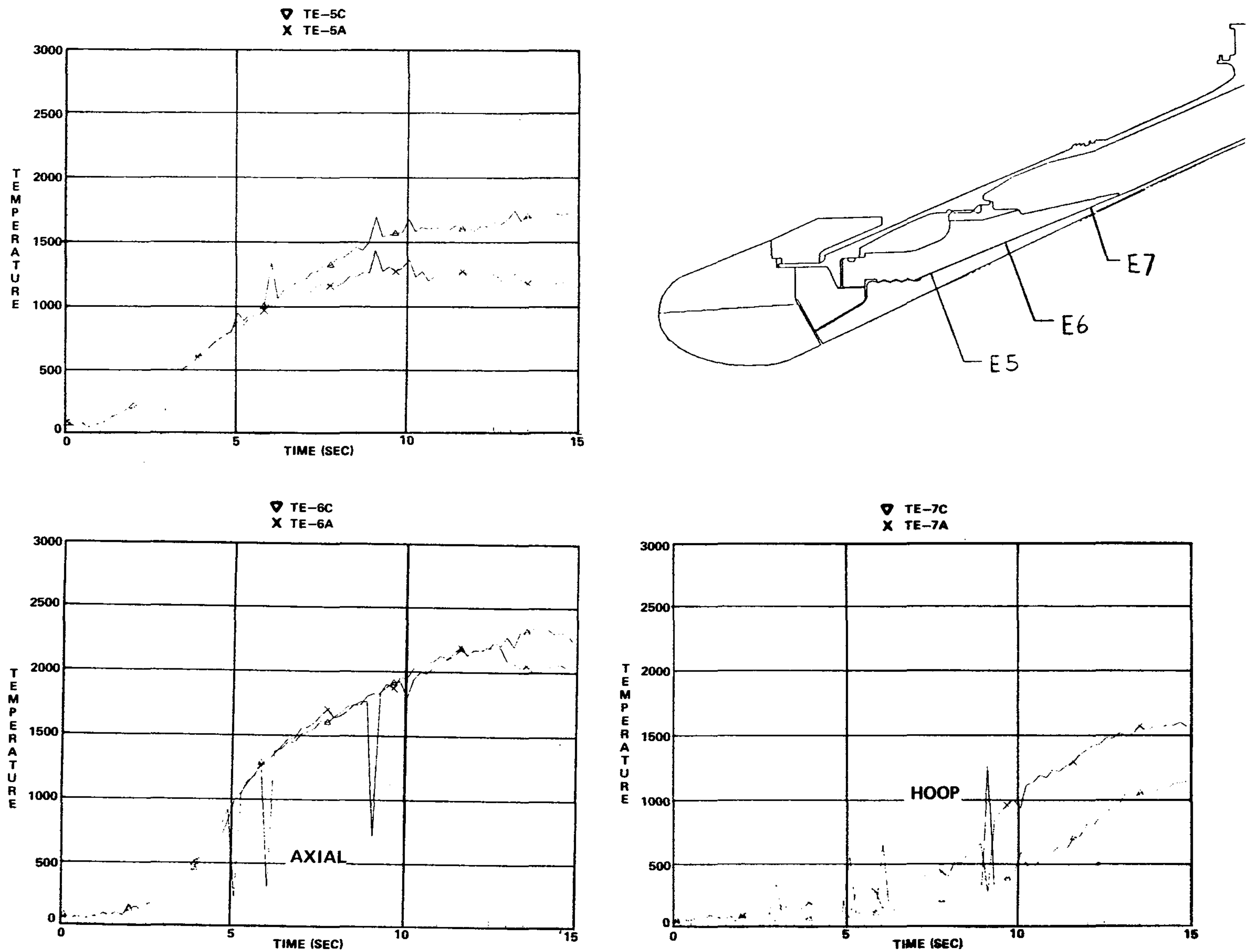
TE–5C
TE–5A
3000
2500
2000
1500
1000
500
0
TEMPERATURE
0
5
10
15
TIME (SEC)
E7
E6
E5
TE–6C
TE–6A
AXIAL
TE–7C
TE–7A
HOOP

Figure B-6.

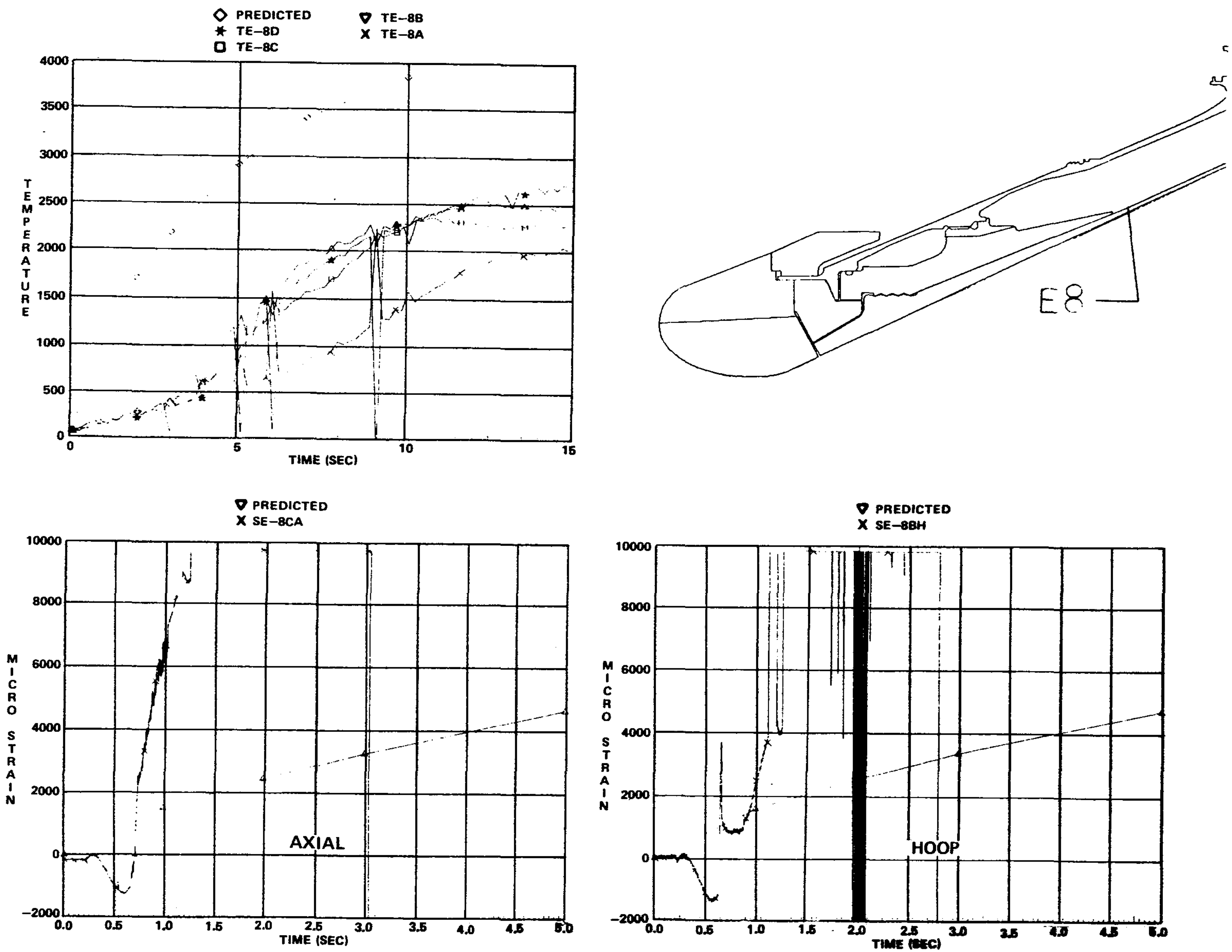
PREDICTED
TE-8D
TE-8C
TE-8B
TE-8A
TEMPERATURE
4000
3500
3000
2500
2000
1500
1000
500
0
0
5
10
15
TIME (SEC)
E8
PREDICTED
SE-8CA
MICRO STRAIN
10000
8000
6000
4000
2000
0
-2000
0.0
0.5
1.0
1.5
2.0
2.5
3.0
3.5
4.0
4.5
5.0
TIME (SEC)
AXIAL
PREDICTED
SE-8BH
MICRO STRAIN
10000
8000
6000
4000
2000
0
-2000
0.0
0.5
1.0
1.5
2.0
2.5
3.0
3.5
4.0
4.5
5.0
TIME (SEC)
HOOP

Figure B-7.

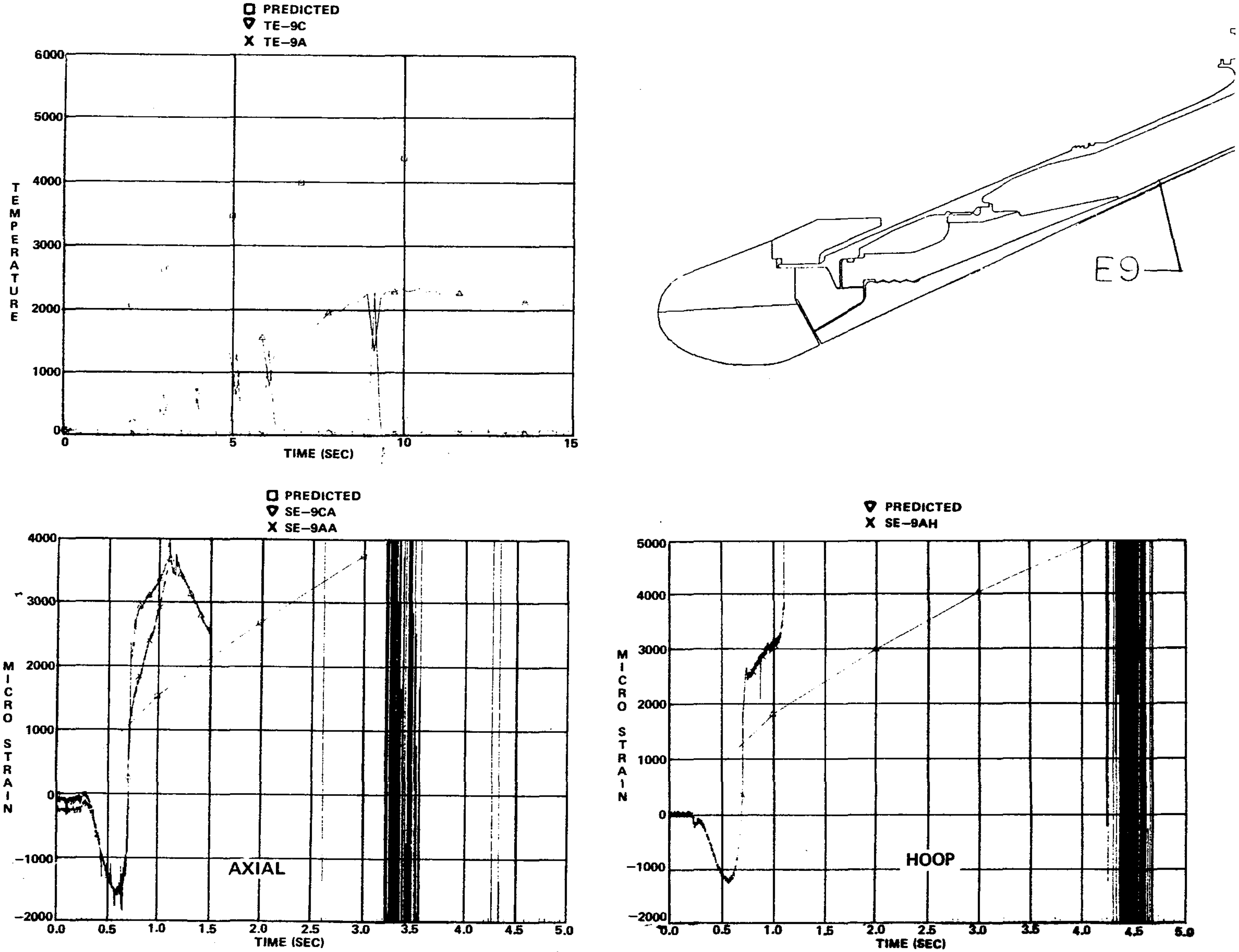
PREDICTED
TE–9C
TE–9A
TEMPERATURE
TIME (SEC)
E9
PREDICTED
SE–9CA
SE–9AA
MICRO STRAIN
AXIAL
TIME (SEC)
PREDICTED
SE–9AH
MICRO STRAIN
HOOP
TIME (SEC)

Figure B-8.

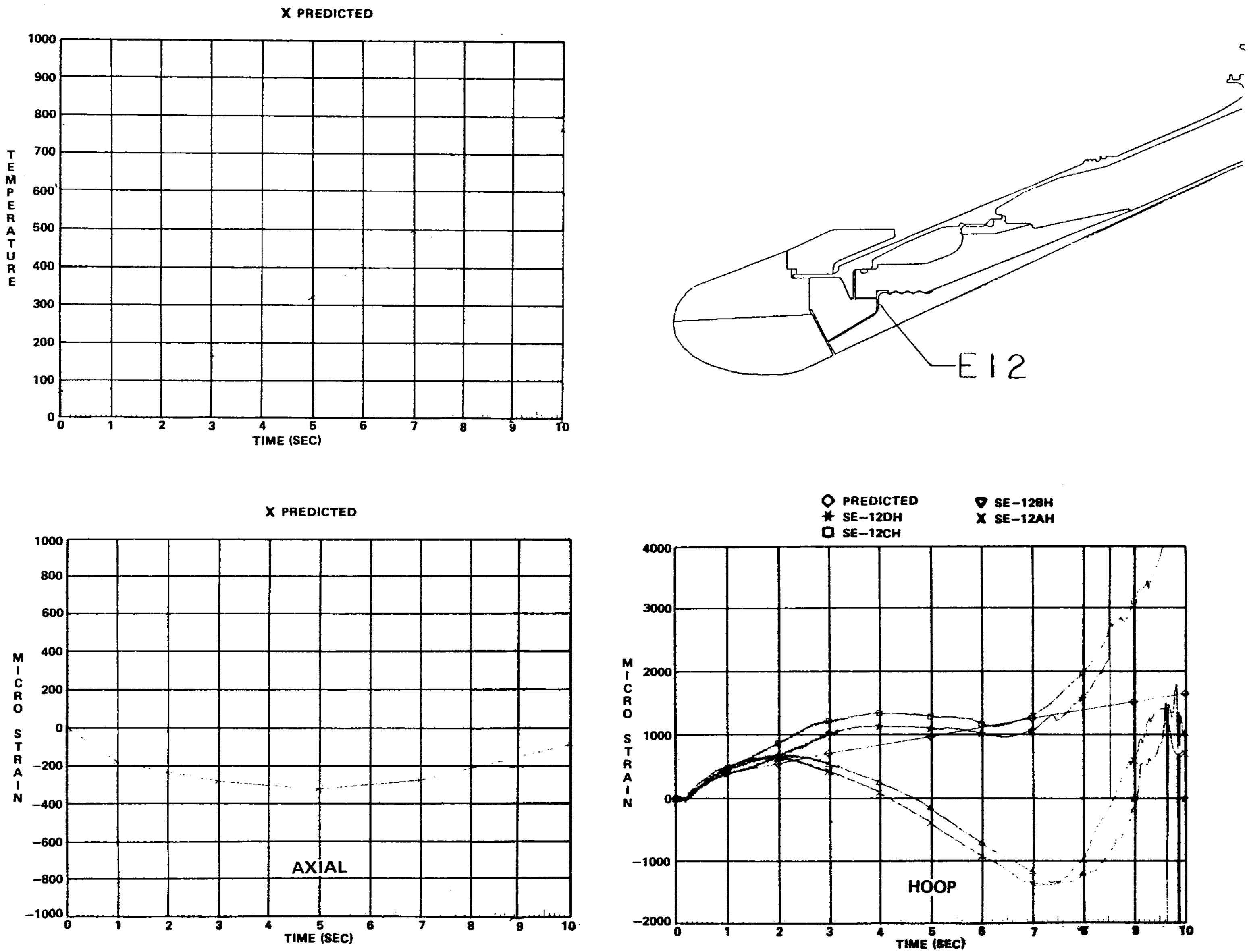
X PREDICTED
TEMPERATURE
TIME (SEC)
E12
X PREDICTED
MICRO STRAIN
AXIAL
TIME (SEC)
PREDICTED
SE-12DH
SE-12CH
SE-12BH
SE-12AH
MICRO STRAIN
HOOP
TIME (SEC)

Figure B-9.

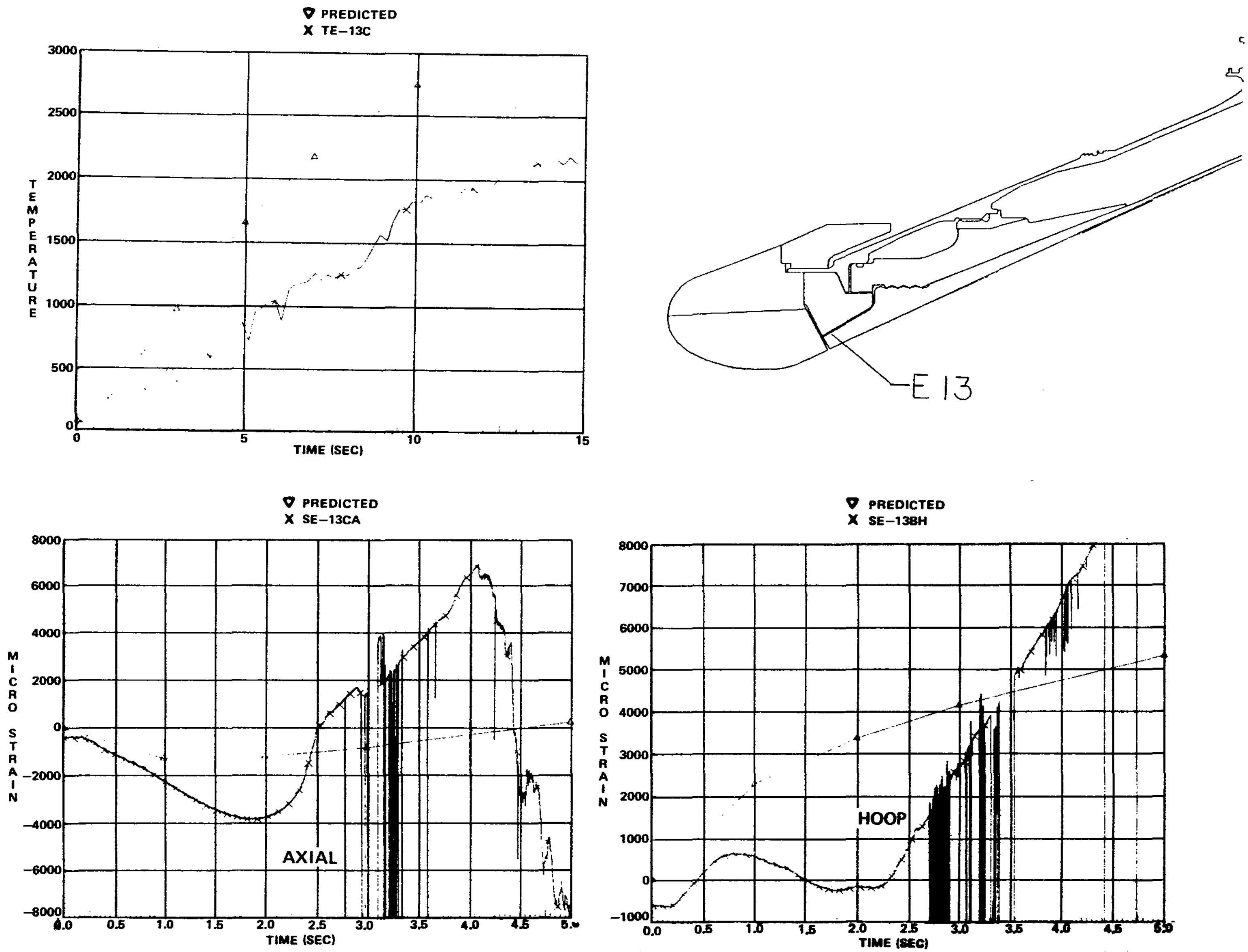

PREDICTED
TE–13C
TEMPERATURE
3000
2500
2000
1500
1000
500
0
0
5
10
15
TIME (SEC)
E 13
PREDICTED
SE–13CA
MICRO STRAIN
8000
6000
4000
2000
0
–2000
–4000
–6000
–8000
AXIAL
0.5
1.0
1.5
2.0
2.5
3.0
3.5
4.0
4.5
TIME (SEC)
PREDICTED
SE–13BH
MICRO STRAIN
8000
7000
6000
5000
4000
3000
2000
1000
0
–1000
HOOP
0.0
0.5
1.0
1.5
2.0
2.5
3.0
3.5
4.0
4.5
5.0
TIME (SEC)


Figure B-10.

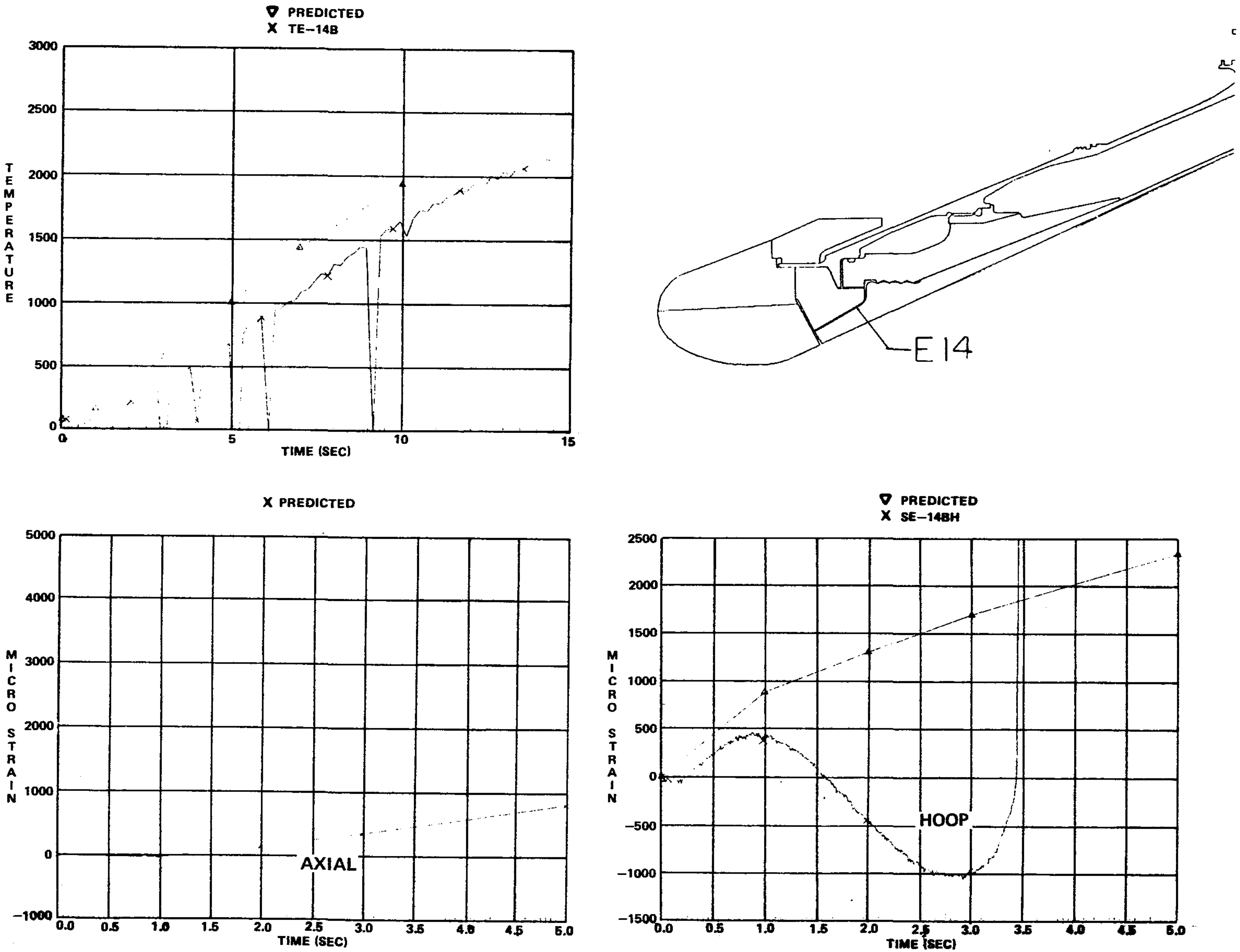

PREDICTED
TE-14B
TEMPERATURE
TIME (SEC)
E14
X PREDICTED
MICRO STRAIN
AXIAL
TIME (SEC)
PREDICTED
SE-14BH
MICRO STRAIN
HOOP
TIME (SEC)


Figure B-11.

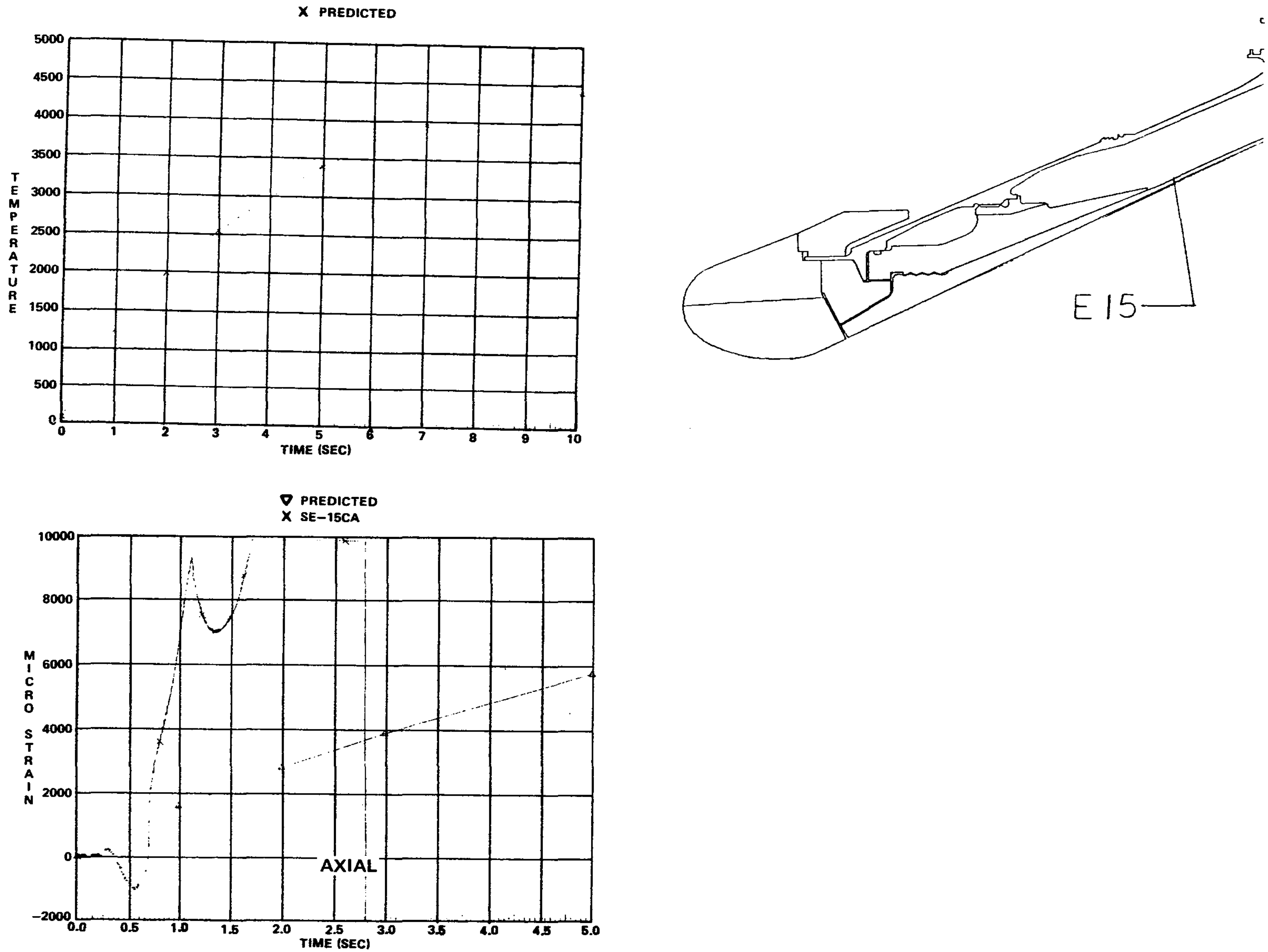

X PREDICTED
TEMPERATURE
0
500
1000
1500
2000
2500
3000
3500
4000
4500
5000
0 1 2 3 4 5 6 7 8 9 10
TIME (SEC)
▽ PREDICTED
X SE-15CA
MICRO STRAIN
-2000
0
2000
4000
6000
8000
10000
AXIAL
0.0 0.5 1.0 1.5 2.0 2.5 3.0 3.5 4.0 4.5 5.0
TIME (SEC)
E15


Figure B-12.

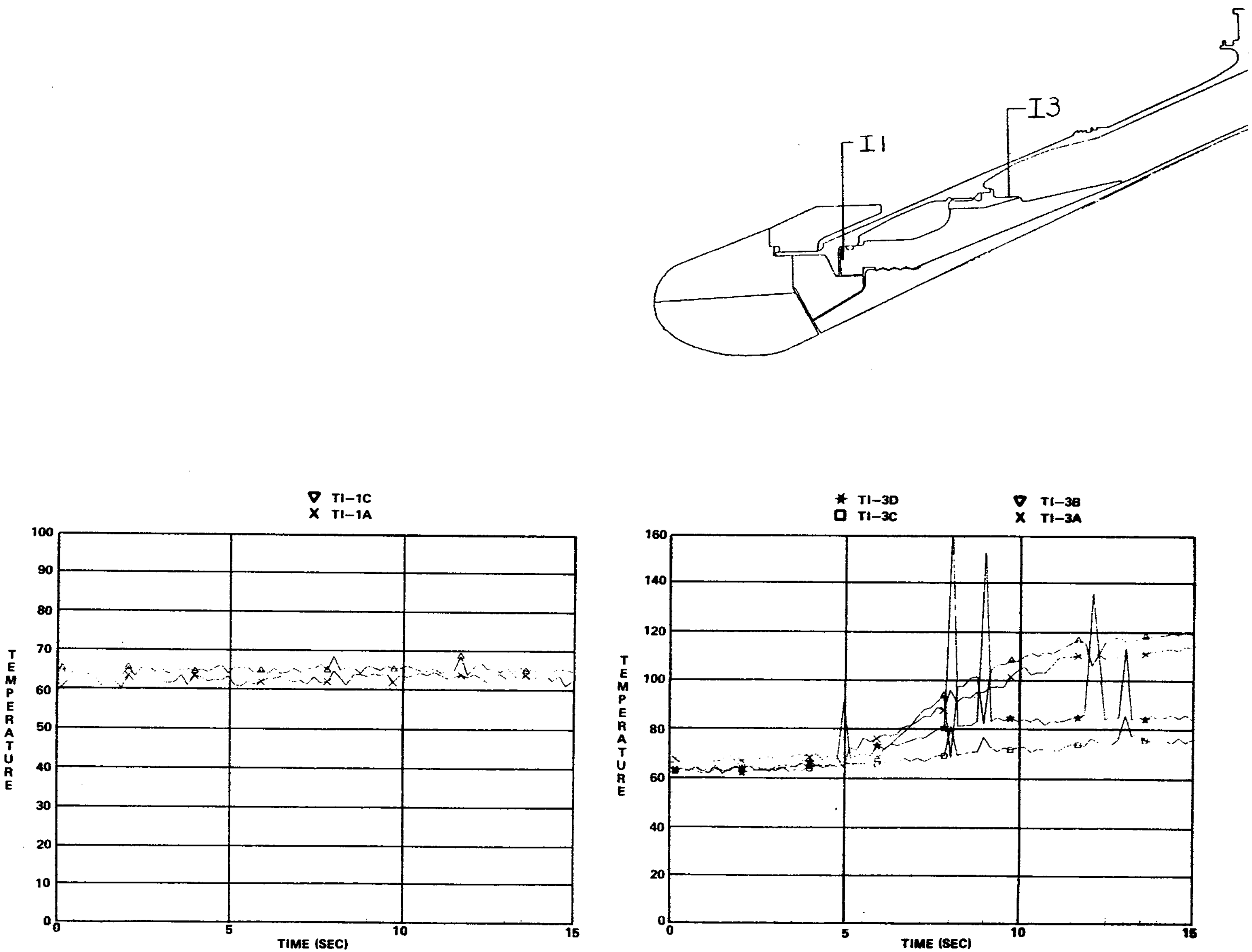
I1
I3
TI-1C
TI-1A
TEMPERATURE
TIME (SEC)
TI-3D
TI-3C
TI-3B
TI-3A
TEMPERATURE
TIME (SEC)

Figure B-13.

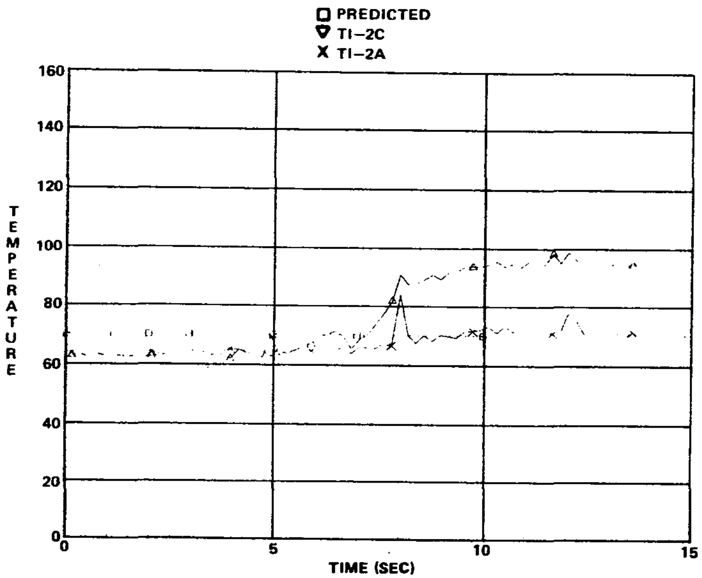
PREDICTED
TI-2C
TI-2A
TEMPERATURE
TIME (SEC)

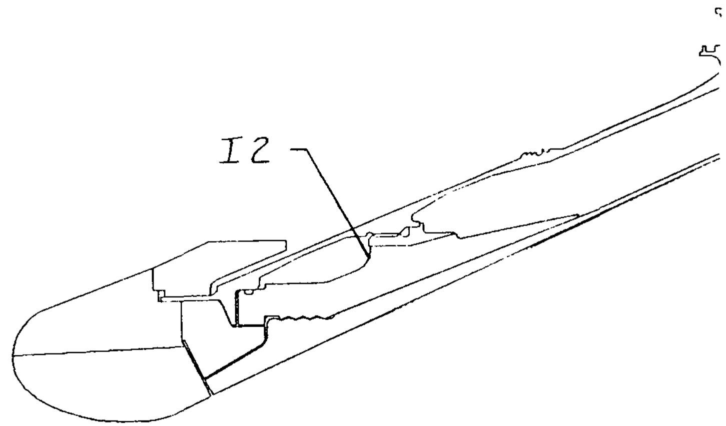
I2

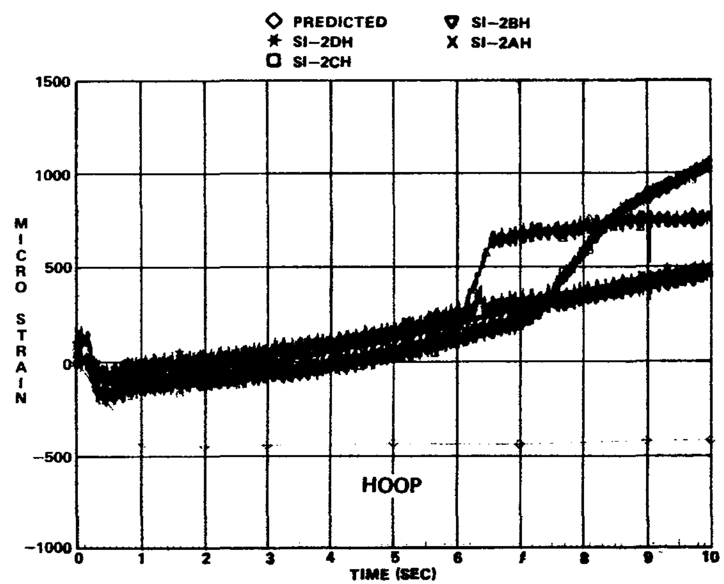
PREDICTED
SI-2DH
SI-2CH
SI-2BH
SI-2AH
MICRO STRAIN
HOOP
TIME (SEC)

Figure B-14.

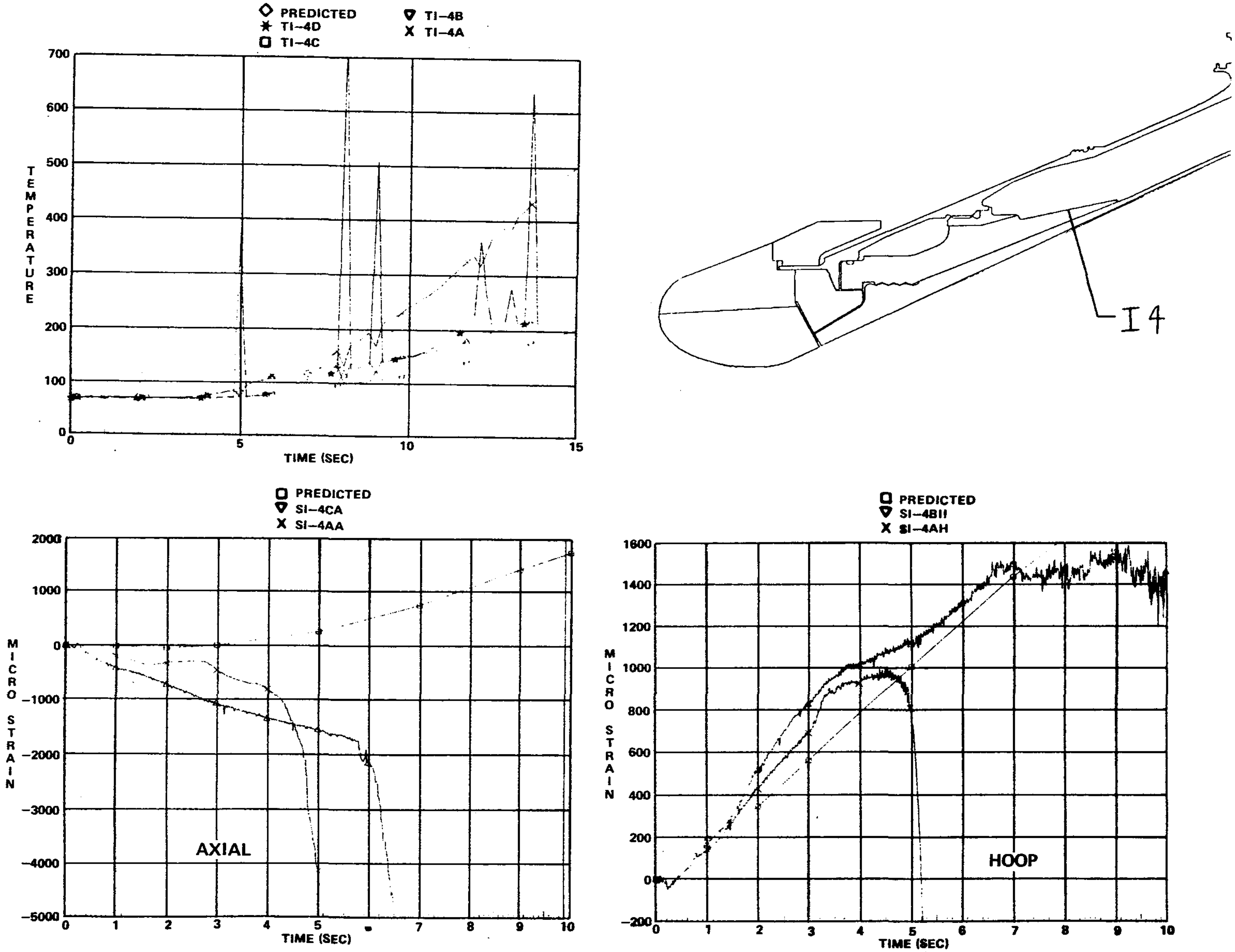
PREDICTED
TI-4D
TI-4C
TI-4B
TI-4A
TEMPERATURE
TIME (SEC)
I4
PREDICTED
SI-4CA
SI-4AA
MICRO STRAIN
AXIAL
TIME (SEC)
PREDICTED
SI-4BH
SI-4AH
MICRO STRAIN
HOOP
TIME (SEC)

Figure B-15.

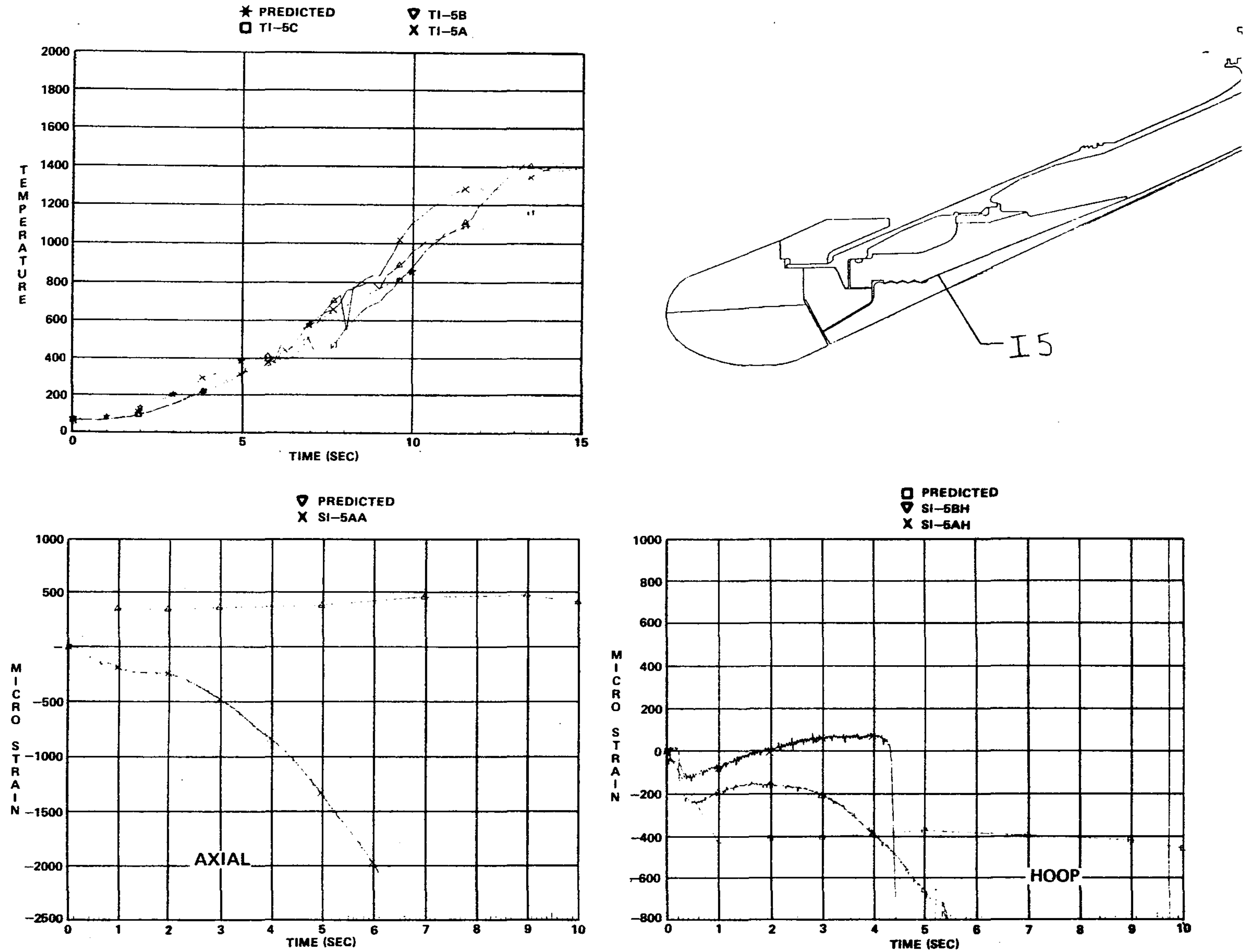
PREDICTED
TI–5C
TI–5B
TI–5A
TEMPERATURE
TIME (SEC)
I5
PREDICTED
SI–5AA
MICRO STRAIN
AXIAL
TIME (SEC)
PREDICTED
SI–5BH
SI–5AH
MICRO STRAIN
HOOP
TIME (SEC)

Figure B-16.

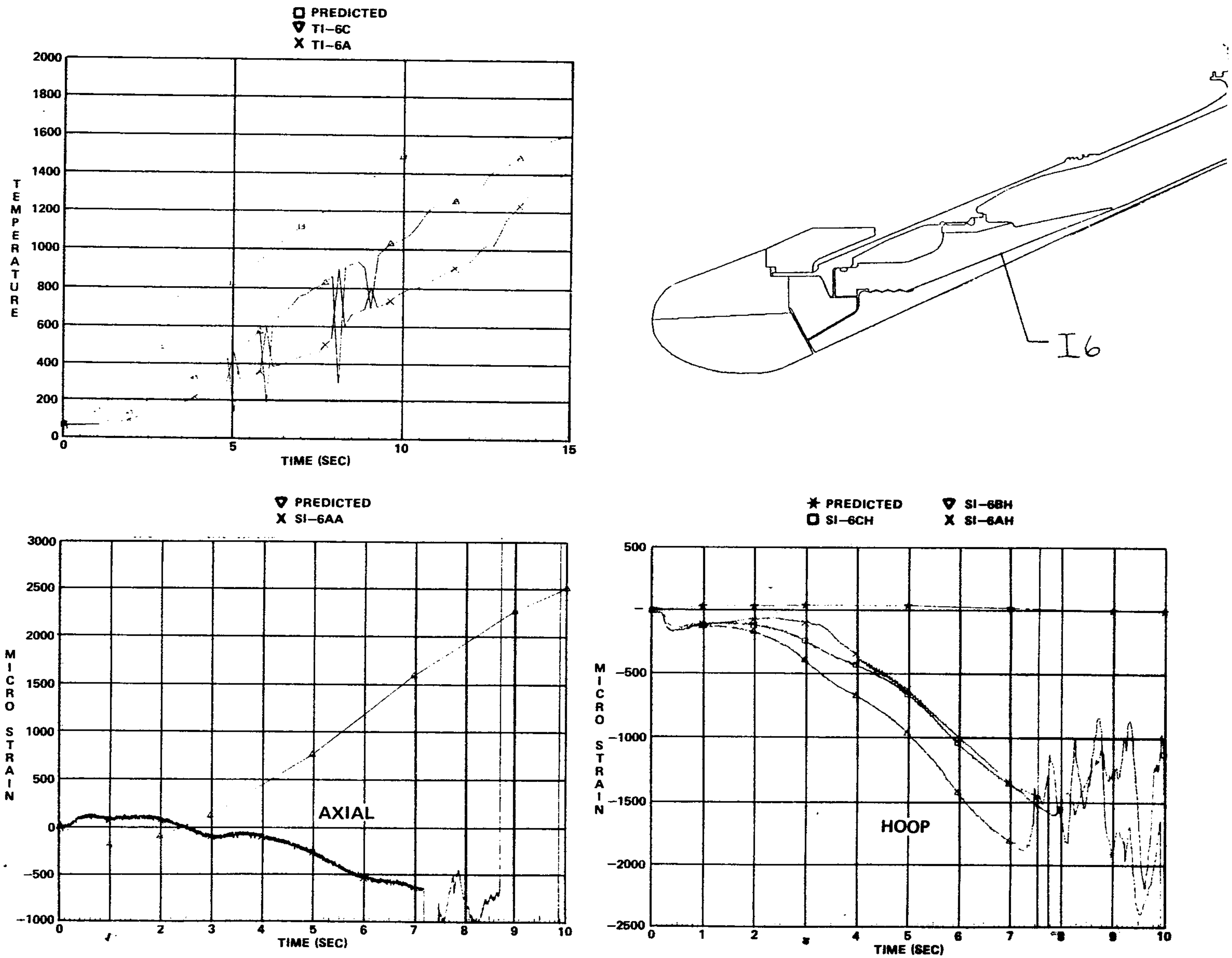

PREDICTED
TI-6C
TI-6A
TEMPERATURE
2000
1800
1600
1400
1200
1000
800
600
400
200
0
0
5
10
15
TIME (SEC)
I6
PREDICTED
SI-6AA
MICRO STRAIN
3000
2500
2000
1500
1000
500
0
-500
-1000
AXIAL
0
2
3
4
5
6
7
8
9
10
TIME (SEC)
PREDICTED
SI-6BH
SI-6CH
SI-6AH
MICRO STRAIN
500
-500
-1000
-1500
-2000
-2500
HOOP
0
1
2
4
5
6
7
9
10
TIME (SEC)


Figure B-17.

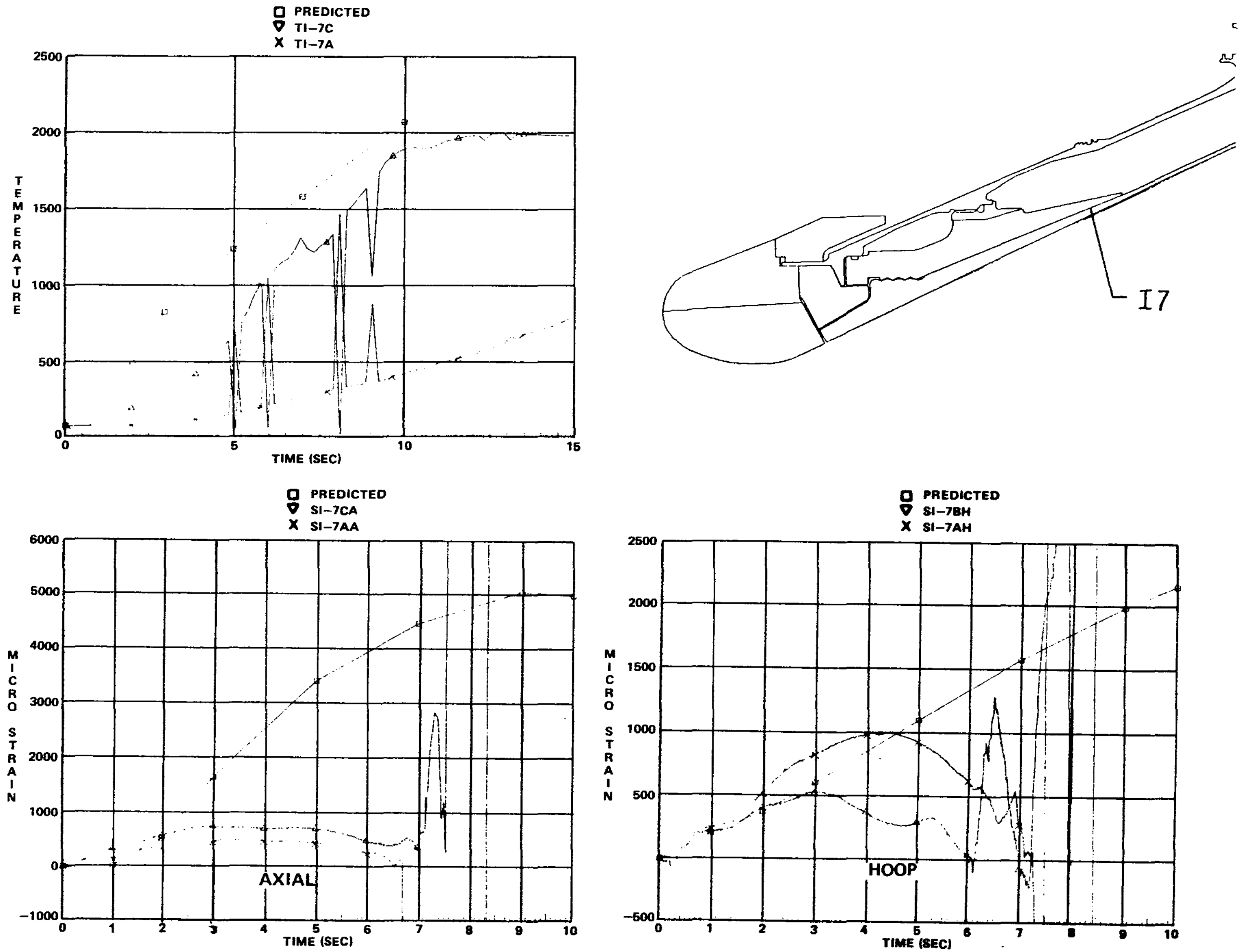
PREDICTED
TI–7C
TI–7A
TEMPERATURE
TIME (SEC)
I7
PREDICTED
SI–7CA
SI–7AA
MICRO STRAIN
AXIAL
TIME (SEC)
PREDICTED
SI–7BH
SI–7AH
MICRO STRAIN
HOOP
TIME (SEC)

Figure B-18.

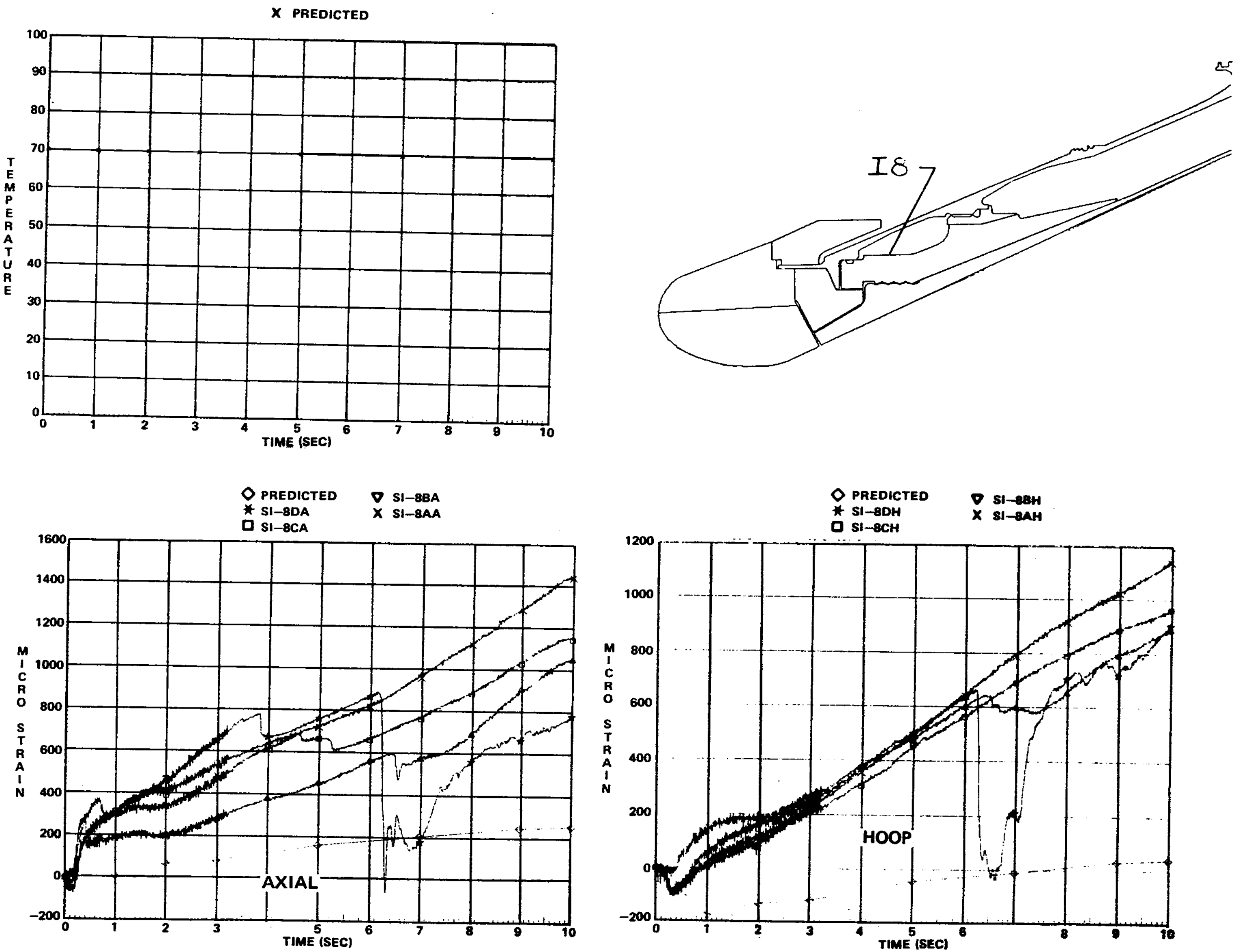
X PREDICTED
TEMPERATURE
TIME (SEC)
I8
◇ PREDICTED
✱ SI–8DA
□ SI–8CA
▽ SI–8BA
X SI–8AA
MICRO STRAIN
AXIAL
TIME (SEC)
◇ PREDICTED
✱ SI–8DH
□ SI–8CH
▽ SI–8BH
X SI–8AH
MICRO STRAIN
HOOP
TIME (SEC)

Figure B-19.

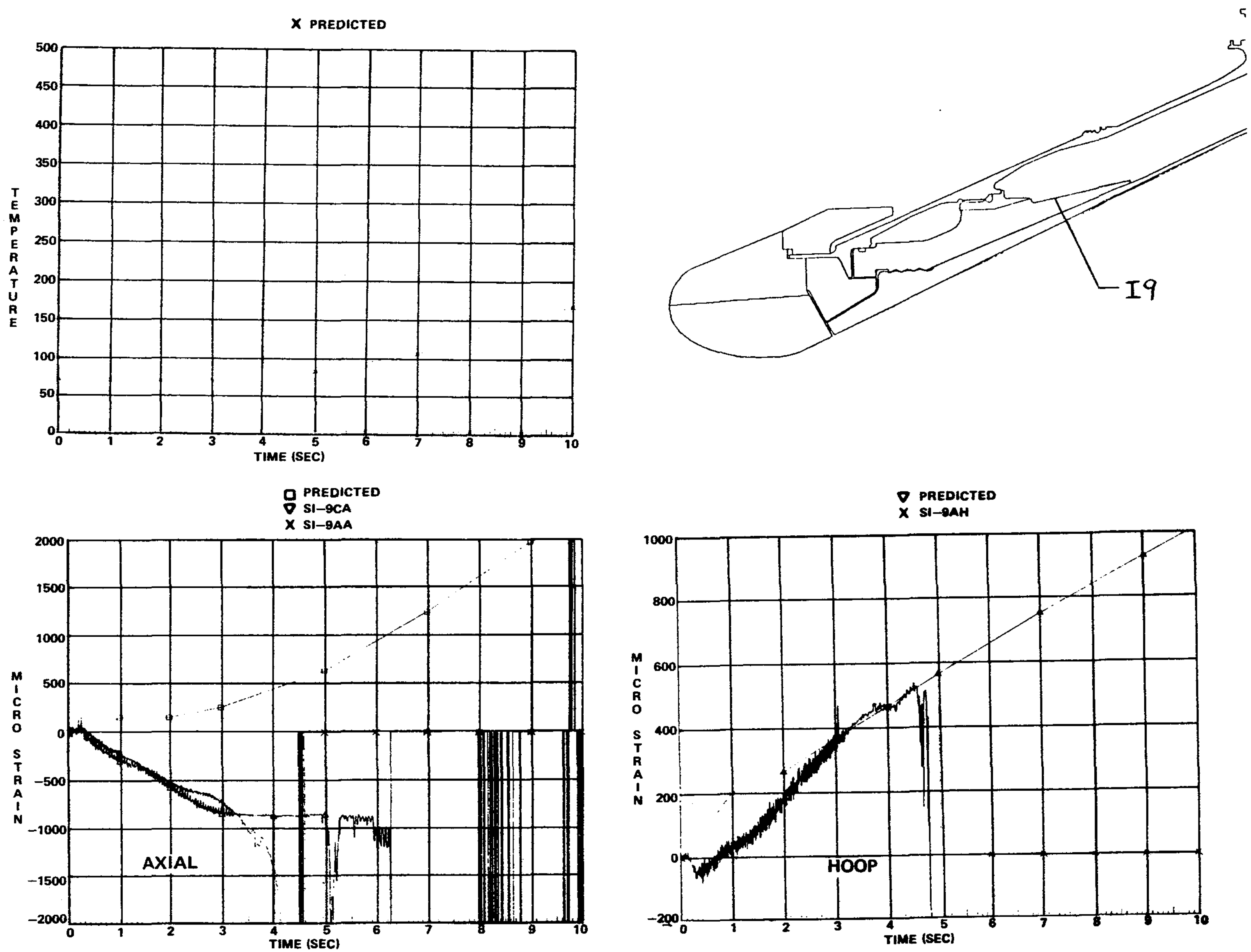
X PREDICTED
TEMPERATURE
TIME (SEC)
I9
□ PREDICTED
▽ SI-9CA
X SI-9AA
MICRO STRAIN
AXIAL
TIME (SEC)
▽ PREDICTED
X SI-9AH
MICRO STRAIN
HOOP
TIME (SEC)

Figure B-20.

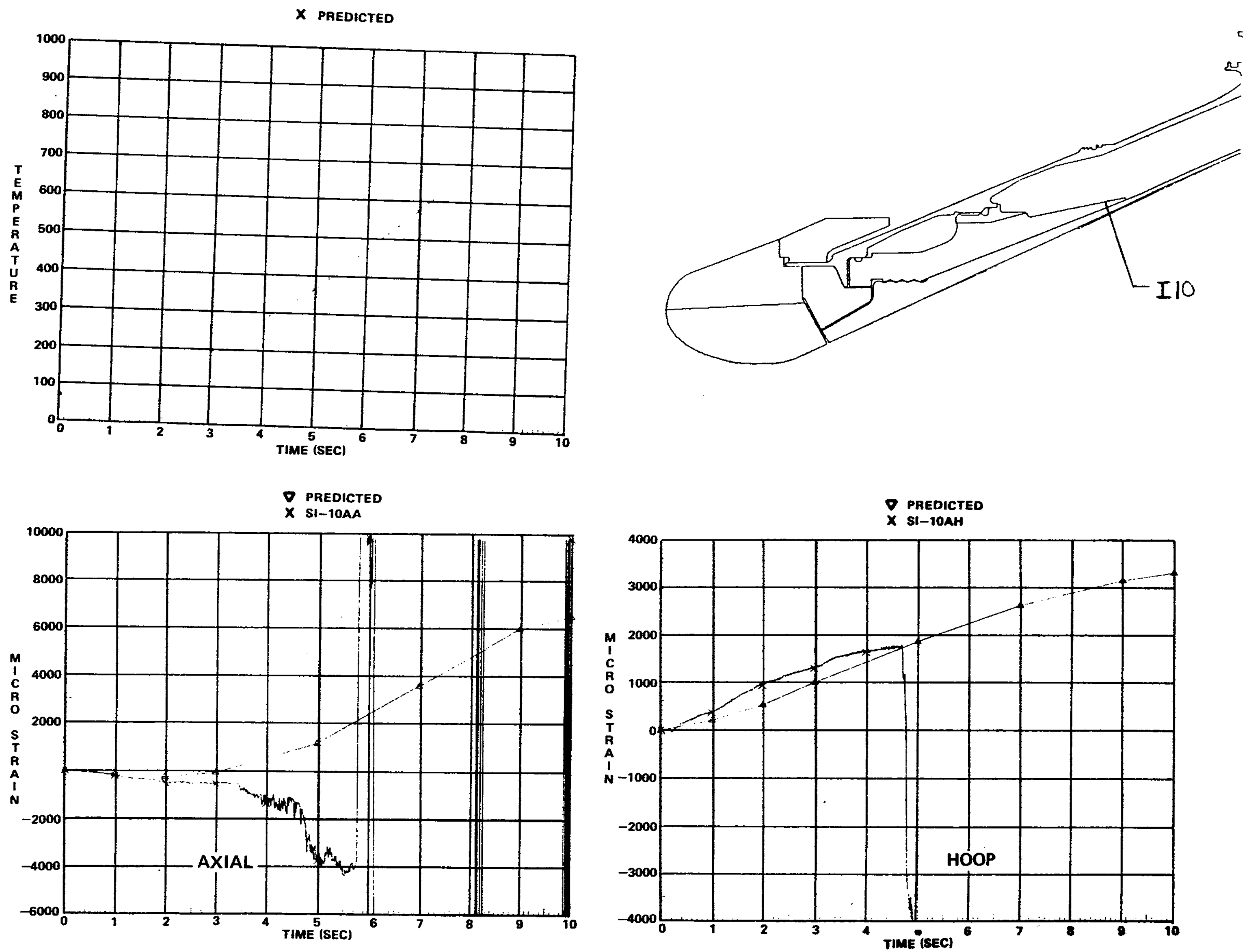
X PREDICTED
TEMPERATURE
TIME (SEC)
I10
▽ PREDICTED
X SI-10AA
MICRO STRAIN
AXIAL
TIME (SEC)
▽ PREDICTED
X SI-10AH
MICRO STRAIN
HOOP
TIME (SEC)

Figure B-21.

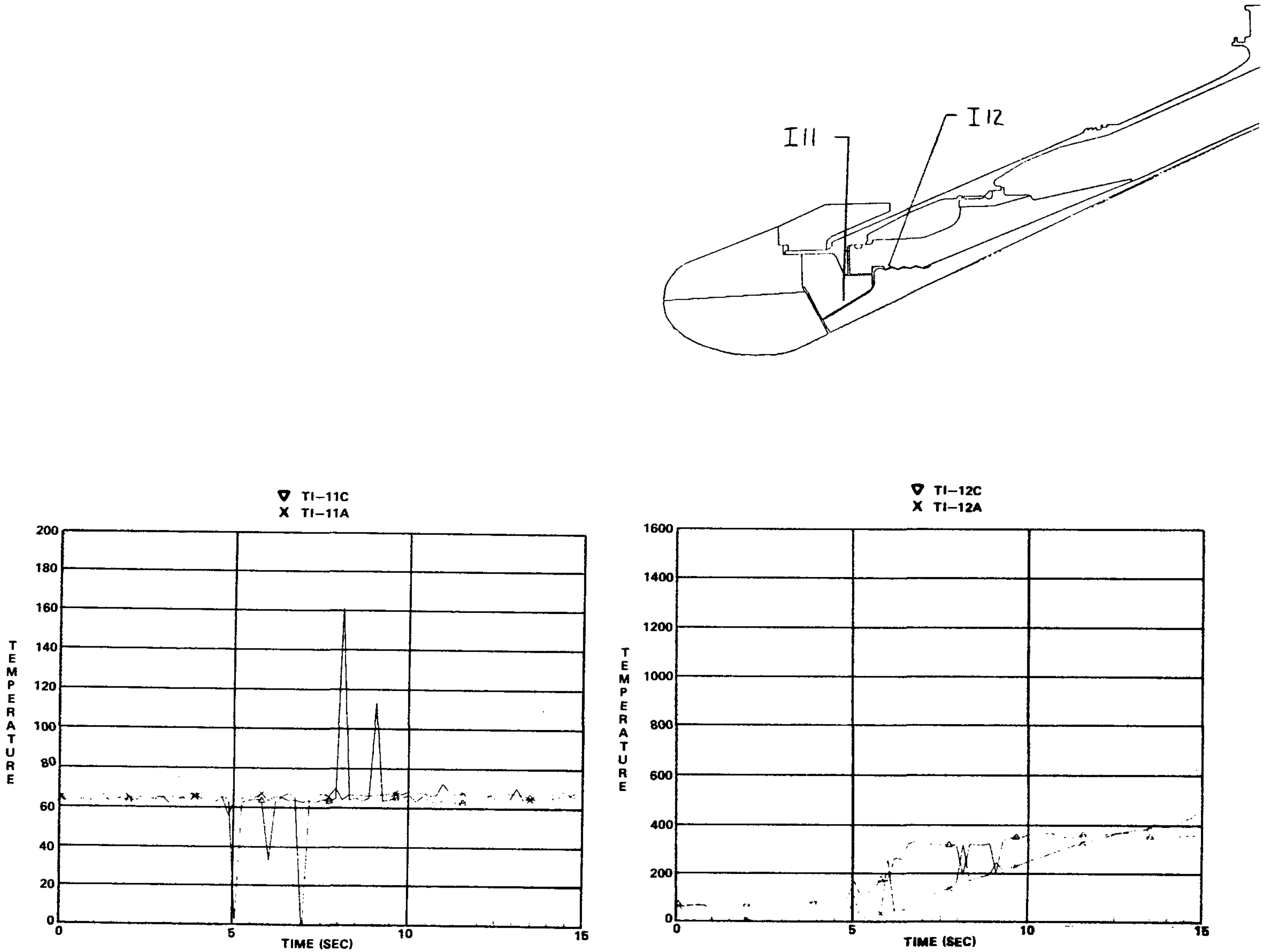
I11
I12
TI-11C
TI-11A
TEMPERATURE
TIME (SEC)
TI-12C
TI-12A
TEMPERATURE
TIME (SEC)

Figure B-22.

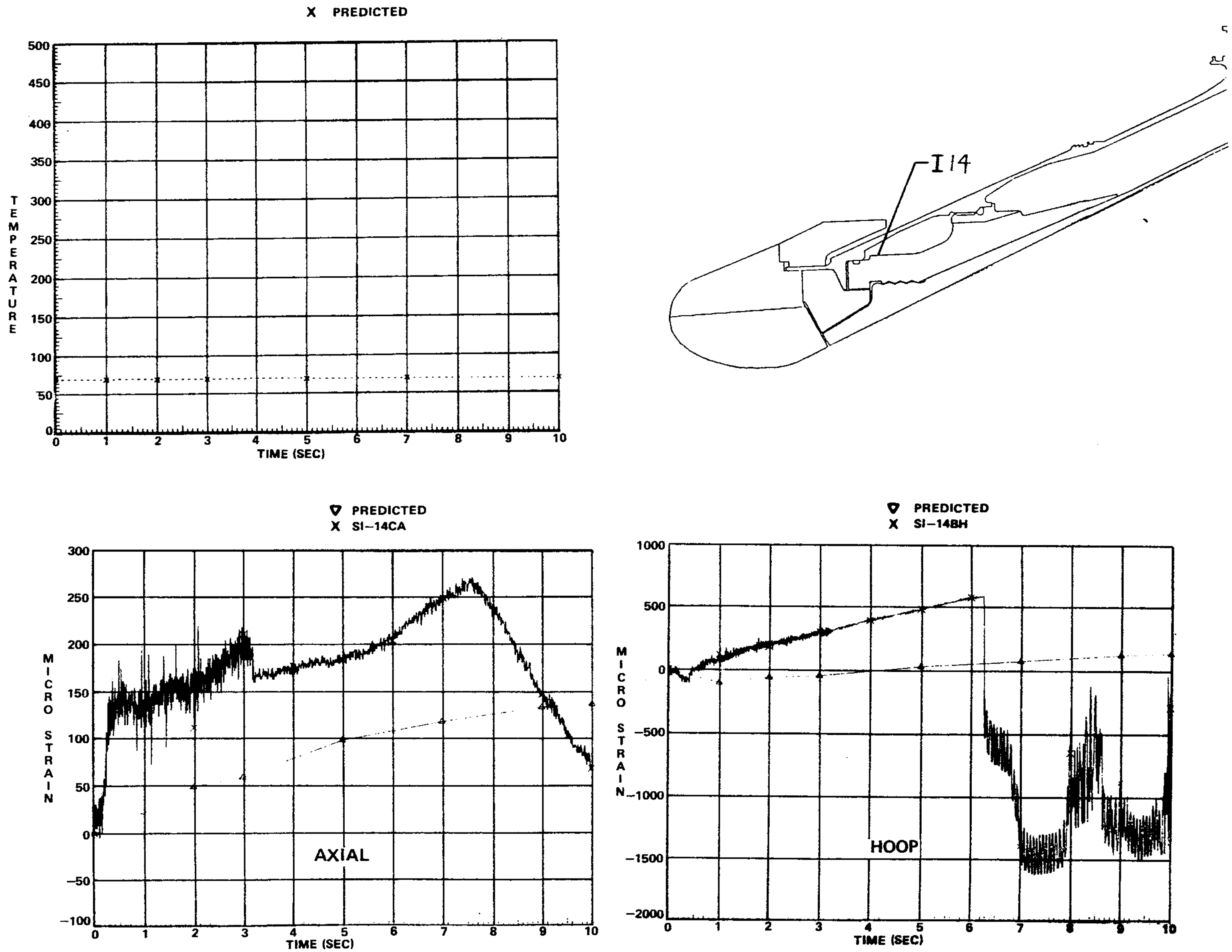
X PREDICTED
TEMPERATURE
TIME (SEC)
I14
▽ PREDICTED
X SI–14CA
MICRO STRAIN
AXIAL
TIME (SEC)
▽ PREDICTED
X SI–14BH
MICRO STRAIN
HOOP
TIME (SEC)

Figure B-23.

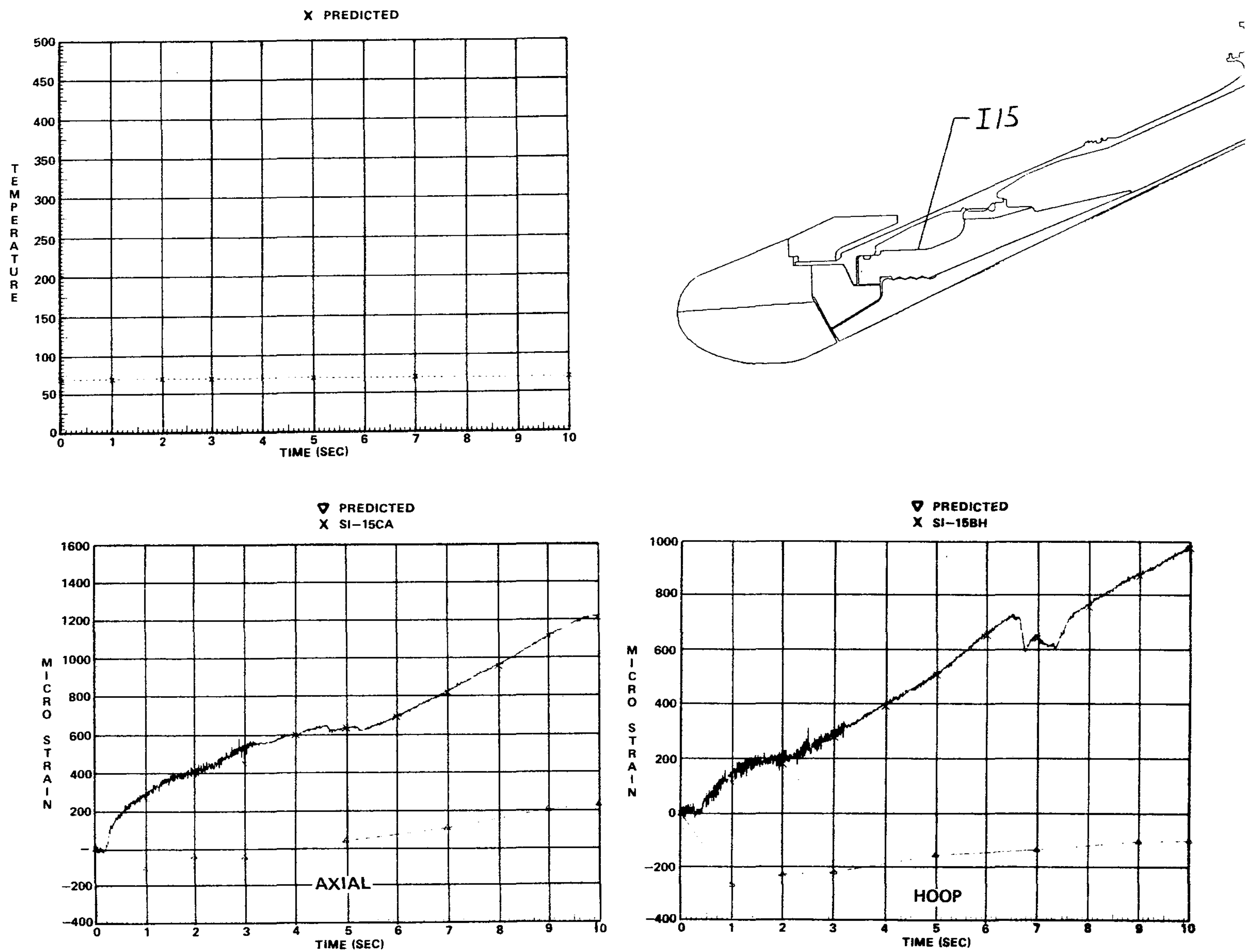
X PREDICTED
TEMPERATURE
TIME (SEC)
I15
▽ PREDICTED
X SI–15CA
MICRO STRAIN
AXIAL
TIME (SEC)
▽ PREDICTED
X SI–15BH
MICRO STRAIN
HOOP
TIME (SEC)

Figure B-24.

| 1. REPORT NO. | 2. GOVERNMENT ACCESSION NO. | 3. RECIPIENT'S CATALOG NO. |
|---|---|---|
| NASA TP -2572 | | |

| 4. TITLE AND SUBTITLE | 5. REPORT DATE |
|---|---|
| Star 48 Solid Rocket Motor Nozzle Analyses and Instrumented Firings | March 1986 |
| | 6. PERFORMING ORGANIZATION CODE |
| 7. AUTHOR(S) Robert L. Porter | 8. PERFORMING ORGANIZATION REPORT # |
| 9. PERFORMING ORGANIZATION NAME AND ADDRESS | 10. WORK UNIT NO. M-515 |
| George C. Marshall Space Flight Center<br>Marshall Space Flight Center, Alabama 35812 | 11. CONTRACT OR GRANT NO. |
| | 13. TYPE OF REPORT & PERIOD COVERED |
| 12. SPONSORING AGENCY NAME AND ADDRESS<br>National Aeronautics and Space Administration<br>Washington, D.C. 20546 | Technical Paper |
| | 14. SPONSORING AGENCY CODE |

15. SUPPLEMENTARY NOTES

Prepared by Structures and Propulsion Laboratory, Science and Engineering Directorate.

16. ABSTRACT

This report presents the analyses and testing performed by NASA in support of an expanded and improved nozzle design data base for use by the U.S. solid rocket motor industry. A production nozzle with a history of one ground failure and two flight failures was selected for analyses and testing.

The stress analysis was performed with the Champion computer code developed by the U.S. Navy. Several improvements were made to the code. Strain predictions were made and compared to test data.

Two short duration motor firings were conducted with highly instrumented nozzles. The first nozzle had 58 thermocouples, 66 strain gages, and 8 bondline pressure measurements. The second nozzle had 59 thermocouples, 68 strain measurements, and 8 bondline pressure measurements. Most of this instrumentation was on the nonmetallic parts, and provided significantly more thermal and strain data on the nonmetallic components of a nozzle than has been accumulated in a solid rocket motor test to date.

| 17. KEY WORDS | 18. DISTRIBUTION STATEMENT |
|---|---|
| Solid Rocket Motor Nozzle | Category No. 15<br><br>Unclassified–U. S. Government agencies and U. S. Government agency contractors only |

| 19. SECURITY CLASSIF. (of this report) | 20. SECURITY CLASSIF. (of this page) | 21. NO. OF PAGES | 22. PRICE |
|---|---|---|---|
| Unclassified | Unclassified | 58 | A04 |

For sale by National Technical Information Service, Springfield, Virginia 22161

NASA-Langley, 1986